

The role of the evaporating microlayer and dry surface areas in boiling

Citation for published version (APA):

Ouwerkerk, van, H. J. (1970). *The role of the evaporating microlayer and dry surface areas in boiling*. [Phd Thesis 1 (Research TU/e / Graduation TU/e), Applied Physics and Science Education]. Technische Hogeschool Eindhoven. <https://doi.org/10.6100/IR133004>

DOI:

[10.6100/IR133004](https://doi.org/10.6100/IR133004)

Document status and date:

Published: 01/01/1970

Document Version:

Publisher's PDF, also known as Version of Record (includes final page, issue and volume numbers)

Please check the document version of this publication:

- A submitted manuscript is the version of the article upon submission and before peer-review. There can be important differences between the submitted version and the official published version of record. People interested in the research are advised to contact the author for the final version of the publication, or visit the DOI to the publisher's website.
- The final author version and the galley proof are versions of the publication after peer review.
- The final published version features the final layout of the paper including the volume, issue and page numbers.

[Link to publication](#)

General rights

Copyright and moral rights for the publications made accessible in the public portal are retained by the authors and/or other copyright owners and it is a condition of accessing publications that users recognise and abide by the legal requirements associated with these rights.

- Users may download and print one copy of any publication from the public portal for the purpose of private study or research.
- You may not further distribute the material or use it for any profit-making activity or commercial gain
- You may freely distribute the URL identifying the publication in the public portal.

If the publication is distributed under the terms of Article 25fa of the Dutch Copyright Act, indicated by the "Taverne" license above, please follow below link for the End User Agreement:

www.tue.nl/taverne

Take down policy

If you believe that this document breaches copyright please contact us at:

openaccess@tue.nl

providing details and we will investigate your claim.

THE ROLE OF THE EVAPORATING
MICROLAYER AND DRY SURFACE
AREAS IN BOILING

H. J. VAN OUWERKERK

**THE ROLE OF THE EVAPORATING
MICROLAYER AND DRY SURFACE
AREAS IN BOILING**

PROEFSCHRIFT

**TER VERKRIJGING VAN DE GRAAD VAN DOCTOR IN DE
TECHNISCHE WETENSCHAPPEN AAN DE TECHNISCHE
HOGESCHOOL EINDHOVEN OP GEZAG VAN DE RECTOR
MAGNIFICUS PROF. DR. IR. A. A. TH. M. VAN TRIER,
HOGLERAAR IN DE AFDELING DER ELEKTROTECH-
NIEK, VOOR EEN COMMISSIE UIT DE SENAAT TE VER-
DEDIGEN OP DINSDAG 15 DECEMBER 1970 DES NAMID-
DAGS TE 4 UUR**

DOOR

**HENDRIK JACOB VAN OUWERKERK
GEBOREN TE ROTTERDAM**

**DIT PROEFSCHRIFT IS GOEDGEKEURD DOOR DE PROMOTOR
PROF. DR. D. A. DE VRIES**

Aan Ria

CONTENTS

	Page:
CHAPTER 1 INTRODUCTION	
1.1. Boiling, its forms and applications	1
1.2. Problems associated with boiling	2
1.3. The boiling curve	2
1.4. Bubble nucleation	5
1.5. The transition to film boiling	7
CHAPTER 2 EXPERIMENTAL EQUIPMENT AND TECHNIQUE	
2.1. Purpose of experiments	11
2.2. Heating surface	11
2.3. Preparation and handling of gold films	11
2.4. Glass prism	13
2.5. Vessel	14
2.6. Electrical supply	15
2.7. Temperature measurements	16
2.8. High-speed film camera	17
CHAPTER 3 BUBBLE GROWTH	
3.1. The different phases of growth of a bubble	18
3.2. The microlayer under a bubble	20
CHAPTER 4 THEORY OF RAPID BUBBLE GROWTH AT A LIQUID-SOLID INTERFACE	
4.1. Statement of the problem	26
4.2. General aspects of rapid bubble growth	27
4.3. The flow field and the formation of the microlayer	38
4.4. The boundary layer problem	40
4.5. Evaporation of the microlayer and bubble growth rate	47
4.6. Analytical solution for a special case, a useful approximation	53

	Page:
CHAPTER 5	APPLICATION OF THE THEORY TO NUCLEATE POOL BOILING
5.1.	Evaporation at the hemispherical surface 62
5.2.	Experimental verification 64
5.3.	Comparison of results with literature 69
5.4.	The end of the phase of rapid growth 71
CHAPTER 6	DRY AREAS AND THE STABILITY OF NUCLEATE AND FILM BOILING
6.1.	Experiments on the transition to film boiling 73
6.2.	Behaviour of dry areas on a thin wire 75
6.3.	Thermal stability of the two boiling mechanisms 84
6.4.	Construction of the boiling curve 85
6.5.	Numerical example 88
6.6.	Limitations of the analysis 90
CHAPTER 7	CONCLUDING REMARKS AND SUGGESTIONS FOR FUTURE WORK 91
SUMMARY	93
SAMENVATTING	96
LITERATURE	99
LIST OF SYMBOLS AND UNITS	102
ACKNOWLEDGEMENTS	105
CURRICULUM VITAE	106

CHAPTER 1

INTRODUCTION

1.1. Boiling, its forms and applications

Heat transfer to boiling liquids is widely applied for two different purposes. On the one hand, the aim can be to evaporate a liquid, as occurs in steam boilers and distillation equipment, on the other hand the boiling liquid is often used as a very effective heat transfer medium. The latent heat of evaporation provides a heat sink or source at a virtually constant temperature for varying heat loads. The domestic use of boiling for cooking purposes is an example, but also the cooling in nuclear reactors for marine propulsion by boiling water and the use of liquid helium in low-temperature experiments.

Historically the literature on boiling distinguishes between pool boiling conditions and those of boiling with forced flow, also called convective boiling. For either purpose mentioned above both types of conditions are used, for example in batchwise and continuous distillation.

A special form of boiling is that of subcooled boiling, which occurs when the temperature in the bulk of the liquid is below the saturation temperature at the prevailing pressure. Vapour is then generated at the heat transfer surface, where the temperature is above the saturation value, and condenses again when it enters the bulk liquid.

Convective boiling is mostly applied in heated tubes. Liquid entering the tube system is heated until subcooled boiling sets in. Further along the tube the temperature in the bulk of the liquid will reach the saturation level. By definition further evaporation is called saturated boiling. The well-known two-phase flow regimes of bubble flow, slug flow, annular flow and mist flow are then usually found in consecutive tube sections. In pool boiling the stationary situation is that of saturated boiling.

1.2. Problems associated with boiling

In the work described in this thesis we have confined ourselves to saturated pool boiling of a pure liquid. When considered from an experimental point of view it is the simplest type of boiling, but this is not an important restriction because the most interesting problems associated with the boiling process occur in all types of boiling. Not all aspects of these phenomena are understood, even when the complications of flow and subcooling are absent.

We exclude the boiling of liquid metals from our considerations. The possibly different behaviour resulting from their high heat conductivity and special wetting characteristics would require separate study.

The problems which stand out amongst those encountered in pool boiling concern the nucleation of individual bubbles, their individual growth and their collective behaviour responsible for the transition from nucleate to film boiling. A fair understanding of nucleation, which was found to occur at the heating surface, resulted from the work of Bankoff¹, Griffith² and others. Although there are theories describing bubble growth in the bulk of a liquid, none existed which dealt with the growth of bubbles nucleating at a solid, plane wall. Most attention is therefore given to this particular aspect, which is dealt with in Chapters 3 to 5. Also, attention is paid to the transition from nucleate to film boiling. This is preceded by the coalescence of vapour bubbles resulting in the formation of dry areas on the heating surface. The role played by these dry areas will be analysed in Chapter 6.

The problems of bubble growth at a solid surface and the behaviour of dry areas could be studied fruitfully by direct observation. For this purpose a transparent heating surface was developed. It was used in combination with a high-speed film camera. A description of the experimental methods used is given in Chapter 2.

1.3. The boiling curve

The complex nature of the behaviour of a pool boiling system has been clearly demonstrated by Nukiyama³. As a heating element he used an

electrically heated wire, which also served as a resistance thermometer. In this way he obtained a heat flux versus superheat* curve of the form shown in Figure 1.3.1, usually referred to as the boiling curve.

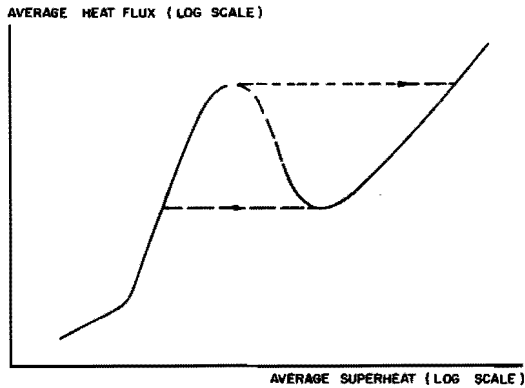


Figure 1.3.1

The boiling curve
Hysteresis for electrically heated systems

At the smallest wire superheats heat transfer is by thermal convection only. Vapour bubbles are not generated until the superheat has reached values in the range of 5 to 10 K. Surface tension effects which govern the nucleation of bubbles at tiny pits in the heating surface can explain this phenomenon, as will be described in Section 1.4.

When actual boiling begins vapour is present in the form of individually nucleated bubbles, and is known therefore as nucleate boiling. At the heating surface heat is transported as latent heat and, more important initially, by bubble-induced convection. The heat flux increases rapidly with superheat. The heat convected to the bulk liquid will also be used ultimately for evaporation, as it enables further growth of bubbles there.

* The term superheat is used to indicate a temperature difference, as commonly encountered in the (technical) language on the subject, i. e. the difference between the local temperature and the saturation temperature at the prevailing pressure.

A photographic study by Rallis and Jawurek⁴ of an experiment similar to that of Nukiyama³, carried out to determine bubble volume and frequency, showed that when the heat flux increases, the latent heat transport becomes the more important and finally the predominant heat transfer mechanism. From these and other experiments it follows that bubble nucleation, which depends strongly on heater material and finish, and bubble growth have an important influence on the shape and position of the boiling curve, especially at high heat fluxes.

Coalescence of vapour bubbles occurs near the heating surface when the nucleate boiling peak heat flux, sometimes called the burnout heat flux, is approached. At this point a continuous film of vapour may suddenly be formed, which in the stationary situation covers the entire heating surface, thermally insulating it from the relatively cool liquid. In equipment operated at a fixed heat flux, such as electrically heated systems, the small heat transfer coefficient associated with this so-called film boiling can lead to an excessive heating surface temperature and damage of the heating surface itself, called burnout. This hazard has a strong influence on the design of boiling water nuclear reactors, as the fuel elements can also be considered to operate at a fixed heat flux.

Film boiling is a stable form of boiling characterized by the formation of large vapour bubbles which are released at regular intervals in a fixed pattern. The vapour-liquid interface of the film is hydrodynamically unstable. It is deformed by what, according to the theory of Rayleigh-Taylor instability, can be described in a first-order approximation as standing waves with a growing amplitude. Actually only the most unstable wave is observed, which bulges between the nodes and splits off bubbles from the film spaced at wavelength intervals. Chang's paper⁵ was the first to point out the role of hydrodynamic stability in film boiling.

When in film boiling the heat flux at the wire is diminished, film boiling is maintained until nucleate boiling can again establish itself at the minimum film-boiling heat flux, sometimes called the Leidenfrost point, which is much smaller than the nucleate boiling peak heat flux. This hysteresis of the transition between nucleate and film boiling is not ob-

served in systems which use a form of heating in which the wall temperature is fixed, as in the case of boiling at a tube heated internally by condensing steam. In that case part of the resulting boiling curve has a negative slope, which part is usually referred to as the region of transition boiling. It can also be found when hot metal is quenched.

1.4. Bubble nucleation

The formation of vapour bubbles in a liquid requires superheating above the saturation temperature at ambient pressure. On account of the surface tension σ the vapour pressure p_v of a small bubble of constant radius r_b is higher than the ambient pressure $p(\infty)$ by an amount of

$$p_v - p(\infty) = 2\sigma/r_b \quad . \quad (1.4.1)$$

Here and in the following we neglect the Kelvin correction which would multiply the above result by $(\rho_l - \rho'_v)/\rho_l$. ρ'_v and ρ_l are the densities of the vapour in the bubble and the liquid, respectively. At moderate pressures ρ'_v is small compared with ρ_l .

Only when $p_v - p(\infty) > 2\sigma/r_b$ a bubble nucleus can grow. For practical purposes the excess pressure $p_v - p(\infty)$ and the superheat $T_1 - T_0$, where T_0 is the saturation temperature at $p(\infty)$, can be related by the modified Clausius-Clapeyron equation for a vapour that behaves as an ideal gas:

$$p_v - p(\infty) = (T_1 - T_0) \frac{\rho_v L}{T_0} \quad , \quad (1.4.2)$$

where ρ_v is the saturation density of the vapour at T_0 , and L the latent heat of vaporization.

Nuclei of the comparatively large size of a few microns, required to explain the observed superheat values in boiling, are not found in the bulk of pure liquids. Only in small pits and scratches of the heating surface are the conditions such that nuclei of the right size can be produced. This is illustrated by the following two observations. In glass vessels which have smooth walls large superheats can inadvertently be obtained before boiling starts, and when boiling starts it does so explosively.

Briggs⁶ generated large negative pressures in water contained in a horizontal capillary which was rotated about a vertical axis. In both cases impurities ultimately cause vapour formation as they promote nucleation.

A systematic analysis of bubble nucleation at a heating surface cavity has been undertaken by Bankoff¹. We shall discuss his findings here. If the cavity in a flat surface is assumed to be conical and the liquid-vapour interface to be perpendicular to the cavity wall, which corresponds to a wetting angle of 90°, the radius of curvature of the interface will first increase with the amount of vapour in the cavity; see Figure 1.4.1. When the interface reaches the circumference of the

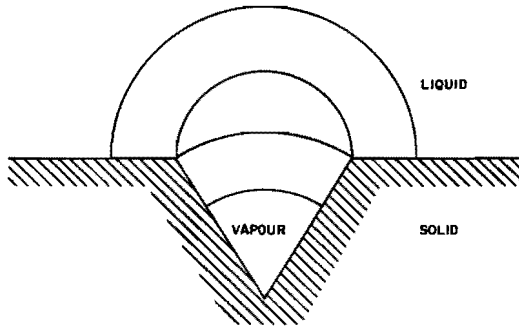


Figure 1.4.1

Nucleation cavity

cavity, it must remain there until it can continue to move, now being perpendicular to the flat surface. Meanwhile the radius of curvature has decreased with increasing vapour volume to the radius r_c of a hemisphere covering the cavity. To be operative this cavity thus requires a superheat of

$$T_1 - T_0 = \frac{2\sigma}{r_c} \frac{T_0}{\rho_v L} \quad (1.4.3)$$

It is assumed that enough gas or vapour is present to ensure that the initial radius of the interface is larger than r_c . This provides another

requirement which a cavity must meet if it is to be an active nucleation centre. Vapour must remain entrapped when the bubbles generated at the cavity leave the heating surface.

Boiling begins when the superheat reaches the value which enables nucleation at the largest cavities which can keep vapour or gas entrapped. At higher superheats increasingly smaller cavities come into action.

It will be shown in Chapter 4 that a growing bubble cools its surroundings to approximately the saturation temperature before it leaves the heating surface. The power input at the surface must then, during the so-called waiting time, restore the lost heat, increasing the temperature to the value at which the cavity can generate the next bubble. As a consequence the initial superheat which determines how that bubble will grow must be practically equal to the value which is specific for the cavity radius given by (1.4.3). We shall argue that in this case it also determines the final bubble size. In general a larger growth rate will lead to a larger final size.

An increase in the heat flux to a boiling liquid and the corresponding increase in wall superheat will thus have various results. More cavities will become operative, larger bubbles will be generated by the newly operative smaller cavities and the waiting times for cavities already operative will be shortened, provided that the number of cavities in operation increases less than proportionally with the heat flux. This will probably occur normally, as the heat flux varies approximately in proportion with the third or fourth power of the wall superheat. See for instance Mc Adams⁷. Convection effects caused by the bubbles may also be important but cannot be predicted.

1.5. The transition to film boiling

Much work has been done in attempts to understand the onset of film boiling or the burnout phenomenon, sometimes with the purpose of providing a basis for the correlation of experimental data. A complete description of this complicated phenomenon has not been given so far.

Some entirely unrelated viewpoints on the cause of burnout have been reported. One concentrates on the hydrodynamics of two-phase flow, another on bubble coalescence. Both will be discussed here. Rohsenow⁸ mentions these and also a third viewpoint which he considers to be equivalent to the second one.

Some years ago, when Zuber⁹ and Chang⁵ tried to explain burnout in terms of hydrodynamic instabilities which might impose a limit on countercurrent transport of vapour and liquid near the heating surface, a breakthrough appeared imminent. However, studies, probably inspired by this work, of pool boiling under conditions of reduced gravity, failed to confirm this theory. These experiments have been discussed by Siegel¹⁰.

Some objections can be raised against the "hydrodynamical viewpoint". If a boiling curve as given in Figure 1.3.1 for a wire also applied to a large flat heating surface, heat fluxes in the film boiling regime could be obtained that are higher than the maximum one observed for nucleate boiling. Thus, the maximum heat flux predicted by a hydrodynamic model should apply to nucleate boiling only, not to film boiling. But the model, which is always formulated as a regular array of vapour channels in the liquid establishing unstable behaviour, offers no suggestion how to incorporate constraints which limit its applicability to nucleate boiling. The important influence of heating surface characteristics - verified experimentally - cannot be incorporated either.

No observations have been reported of the channel-type of flow of the hydrodynamic model. When air is bubbling from a perforated plate through a layer of water supported upon it, a situation is created which is similar to that existing in a boiling liquid. Beek¹¹, in an air-water simulation study of this kind, was the only one to find regular patterns of vapour transport, but the mechanism observed here was entirely different from that corresponding to the hydrodynamical model. Eddies in the liquid transport the vapour in the form of isolated bubbles which are released at positions spaced at regular intervals at the upper surface of the liquid.

The second approach to explain the transition to film boiling concentrates on the role of the coalescence of vapour bubbles. According to this viewpoint the bubble density is important. As the density of active sites for bubble nucleation, and also the product of repetition rate and final bubble volume for a given site, increase with increasing superheat the vapour coverage of the heating surface will also increase. Some authors consider a maximum possible vapour coverage of the heating surface as the cause of transition to film boiling.

Some successful qualitative predictions are based on this viewpoint. Adding small amounts of volatile material to a liquid, Van Wijk, Vos and Van Stralen¹² found a large increase of the nucleate boiling peak heat flux. The concentration at which the peak heat flux occurs coincides with the concentration where the bubble growth rate is strongly reduced. See Van Stralen¹³. The reduction in growth rate is caused by diffusion limitation of the transport in the liquid of the volatile component to the bubble, an effect which has been calculated by Scriven¹⁴. Apparently the tendency to coalesce and the degree of vapour coverage of the heating surface are decreased by the lower bubble growth rate. The second result agrees with our views concerning the end of the phase of bubble growth and final bubble size which are presented at the end of Chapter 5. The Marangoni effect which can promote or inhibit coalescence may also play a role, as has been indicated by Hovestreydt¹⁵. According to the theory of the Marangoni effect the liquid between two approaching bubbles is depleted of volatile component. When the less volatile component has a higher surface tension, contraction of the bubble surfaces will occur locally and liquid is drawn between the bubbles, decreasing the possibility of coalescence.

A quantitative description of the coalescence of bubbles is not available. The importance of coalescence for the transition to film boiling was demonstrated in the papers of Gaertner¹⁶ and of Kirby and Westwater¹⁷. They reported the detection of large vapour mushrooms near the heating surface. Kirby and Westwater¹⁷ also used a glass heating surface and observed the intermittent presence, as we did later, of dry areas on the heating surface. But in spite of these direct observations of the role played by coalescence in the transition to film boiling this problem could not yet be described in a qualitative way.

A study of dry area behaviour has provided us with the means for a first analysis of the influence on the transition to film boiling of the thermal properties of the solid. In a natural way the arguments lead to a discussion of the stability of nucleate and film boiling, as advanced in Chapter 6.

Dry area behaviour has also been analysed by Semeria and Martinet¹⁸, but the relation between this problem and the stability of boiling regimes has never been noticed. Stability was studied by Kovalev¹⁹, who concluded incorrectly that nucleate boiling would be unstable above a certain value of the heat generation, while film boiling would be unstable below this value. Using a different interpretation of the boiling curve to describe the heat transfer to a boiling liquid, different conclusions, involving three values of the heat flux which govern stability, will be drawn in Chapter 6.

CHAPTER 2

EXPERIMENTAL EQUIPMENT AND TECHNIQUE

2.1. Purpose of experiments

To study the transition to film boiling we developed a transparent heating surface allowing direct observation of the phenomena occurring in the boiling liquid in its vicinity. This equipment also enabled us to study the growth of individual bubbles. The experimental techniques are described in this chapter, the results will be discussed in Chapters 5 and 6.

2.2. Heating surface

As the bottom plate for our experimental vessel we used a round plate of 20 mm thickness, made of fused quartz or pyrex glass and for one special experiment of perspex. This plate, which had a diameter of 200 mm, carried on the surface in contact with the liquid a transparent electroconductive layer in the form of a square with sides of 90 mm, which could be heated by passing through an electric current.

In most cases the surface of the plate was ground with a fine grain (amaryl 302) before the layer was applied. This was done to allow the detection of dry areas on the surface of the plate during boiling. A square grid of black dots 10 mm apart was usually painted on the film with India ink as reference length for the measurements. As the refractive indices of the plate and the liquids under investigation were practically equal, the grain on the surface was invisible at places where the liquid was in contact with it, but showed where the surface was dry.

2.3. Preparation and handling of gold films

The transparent electroconductive layer on the glass plate which was used as a heating surface consists of a layer of gold having a thickness of 10 nm, sandwiched between two layers of bismuth oxide with a thickness of 45 nm each, deposited on the glass by evaporation under vacuum.

The purpose of the bismuth oxide layers is to prevent the loss of the originally continuous structure of the gold layer. Without these layers recrystallization of the gold, which adheres poorly to glass-like surfaces, would have this effect. The result is a layer with a low electrical resistance, about 6Ω for a square with contacts along two opposing sides. By evaporation of the metal in the chamber of the vacuum evaporation apparatus a layer of bismuth is deposited on the entire surface of the plate. This layer is oxidized by operating a glow discharge in the presence of some oxygen for about fifteen minutes. Extending from the desired transparent square to the edges of the plate two contacts of the width of the square are formed by the deposition of a thick layer of gold with the use of masks. When another mask has been mounted on the plate, the gold layer of 10 nm is deposited rapidly, i. e. within thirty seconds. Rapid deposition promotes the formation of a layer having a continuous structure. The second layer of bismuth is then deposited on top of the layer of gold without delay, as it is not necessary to reopen the vacuum chamber. Finally oxidation of this second layer is achieved in the way described above.

The properties of the electroconductive layer on a finely ground glass surface are not markedly different from those of a layer on a polished surface.

In electrically conducting liquids we found that the layers dissolved rapidly, which is not surprising considering that the heating voltage is approximately 80 V. We therefore restricted ourselves to n-heptane, benzene and carbon tetrachloride as boiling liquids in the experiments.

With a surface prepared in this manner no difficulties were encountered in bubble growth experiments at a low heat input. In the experiments on the transition from nucleate to film boiling, however, after a certain plate had been in use for some time and the transition had occurred some twenty to thirty times, a tendency developed for the transition to set in at a fixed position.

When the dry area associated with burnout was allowed to cover approximately 20% of the heating surface area, the plates failed, burning away along a narrow path crossing the gold film between the contacts.



Figure 2.4.1

Boiling vessel with glass prism
against transparent heating surface

The uniform colour of the film in reflected light indicated that the total film thickness was constant within 5 nm. As a result of the evaporation technique the gold film thickness will be a constant fraction of the total, and therefore constant within approximately 0.6 nm. The more important point, whether the electrical resistance and hence the temperature and heat generation when supporting boiling, were uniform could not be verified as we saw no easy way to do this without the risk of damaging the films. Moreover, we felt confident about the visual test, while we were certain that the great care taken during manufacture had provided the best gold film we could hope to obtain. Allowance must therefore be made for some uncertainty in the local superheat values in our bubble growth experiments.

2.4. Glass prism

The glass plate was used as a heating surface in our boiling experiments with a glass prism placed against its outer surface. The presence of some glycerol ensured optical contact between plate and prism (Fig. 2.4.1).

A thin film of liquid, extending over an area with dimensions large compared with the film thickness, present on the surface of the plate covered by the electroconductive layer, has its vapour-liquid interface practically parallel to that surface. Diffuse light which enters this film from the vapour is confined to a cone by the "reversed" effect of total reflection. As the refractive indices of liquid, plate and prism are practically equal, the light is confined to the same cone in the prism. When, in the case of visual or photographic observation through a slanted face of the prism, the direction of observation lies outside this cone, the area on the glass plate covered by the liquid film will be observed as a dark area.

Figure 2.4.2 illustrates this situation.

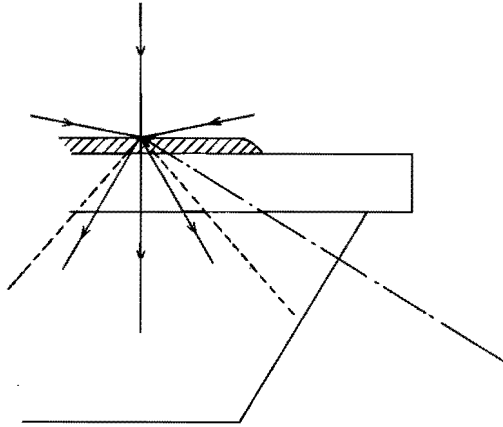


Figure 2.4.2

Glass prism. Reversed effect of total reflection
to detect presence of thin liquid layers

This effect, together with the use of a ground surface, enabled us to observe a liquid microlayer and a dry area at its centre under a vapour bubble growing at low pressure. Similarly, in our study of the burnout phenomenon, the presence of large vapour masses near the heated surface and the occurrence of dry areas on it could be detected.

2.5. Vessel

The boiling vessel consisted of a glass cylinder, a brass top plate and the glass bottom plate already described. Two aluminium rings fitting around the top and bottom plates were connected by four steel rods and pressed the plates against the cylinder, which had a diameter of 150 mm and a height of 250 mm. The plates had a larger diameter than the cylinder. An airtight seal was obtained by placing flat rubber rings (Viton) between cylinder and plates. On the edge of the bottom plate extending outside the cylinder large clamps were placed and pressed against the gold contacts extending from the electroconductive layer. Wires supplied the heating current to these clamps.

To condense the vapour generated by the boiling process, cooling water was passed through brass tubing wound into a helix soldered to the top plate. The large amount of light necessary for the use of a high-speed film camera was supplied by a 1000 W quartz-iodine lamp, supported by stiff electrical wire and submerged in the boiling liquid 30 mm above the heated surface. It was turned on only when the camera was started to prevent the creation of a circulation in the liquid by boiling at the lamp. Where the electrical wires left the vessel, they were soldered to small tubes embedded in a glass bead in a metal ring. This ring was screwed to the top plate and sealed with a rubber "O" ring (Viton). Similar glass beads were used for passing thermocouples into the vessel.

Pressure regulation inside the vessel was done by connecting a brass tube, soldered to the top plate, to the low-pressure side of a reducing valve which was also connected to a vacuum pump. Atmospheric air entered the valve at the high-pressure side and was pumped away at the low-pressure side by the vacuum pump. The reference pressure at the other side of the membrane of the reducing valve was the end vacuum of a second vacuum pump. In this way the pressure could be set at any value below atmospheric pressure. This was important for the study of bubble growth at low pressure and of the dependence of the burnout heat flux on pressure.

2.6. Electrical supply

The heating current, which was direct current in all experiments except one, was taken from batteries, from a Delta Electronics 50 V - 10 A regulated supply, or from a high-power regulated supply built for our requirements at our laboratory. In the latter apparatus a Hall multiplier made it possible to read directly on a recorder the power generated at the heated surface. Supply from batteries was necessary for those experiments on bubble growth comprising time-dependent temperature measurements with small thermocouples and a high-gain oscilloscope amplifier.

2.7. Temperature measurements

Chromel-alumel thermocouples consisting of two wires of 0.05 mm diameter in a stainless steel jacket of 0.35 mm diameter were used for the temperature measurements. The temperature at the centre of the heated surface was measured in a hole drilled in the glass plate and extending almost to the surface in contact with the boiling liquid. The cold junction was immersed in the liquid. The thermocouple voltage of $40 \mu\text{V}$ per K was determined with a Keithley 144 electronic microvoltmeter. The junction of the thermocouples was made by spot-welding the wires at a point extending about 0.40 mm from the jacket. Their rapid response (response time about 2 ms) made it possible to do time-dependent temperature measurements in the vicinity of growing bubbles using a high-gain amplifier and a Tektronix 535 oscilloscope. A sudden drop of the temperature of the junction to a constant value was observed each time a bubble grew at a nearby nucleation centre. This could be shown to correspond to the difference in the temperatures of the superheated liquid surrounding the bubble and the vapour inside, which is at the saturation temperature. The voltage change corresponding to the temperature drop started the time basis of the oscilloscope. An auxiliary voltage which undergoes a step change when the time basis starts, delayed over a chosen time interval by a delay line available in the oscilloscope, was used to actuate a relay through an emitter-follower. The mechanical relay triggered an electronic flashgun, exposing the film in a camera focussed on the thermocouple junction. On a simultaneous photograph of the oscilloscope trace a spike indicates the moment when the flash gun fired. This is illustrated by three photographs, which show that the drop in temperature corresponds to the moment when the junction enters the growing bubble (Figure 2.7.1). In the figure the temperature drop itself is not clearly visible as it triggered the time basis.

Using the saturation temperature as a reference, we then had a technique to measure the temperature of the liquid surrounding a bubble just outside the thermal boundary layer in which the temperature drops to the saturation temperature at the vapour-liquid interface.

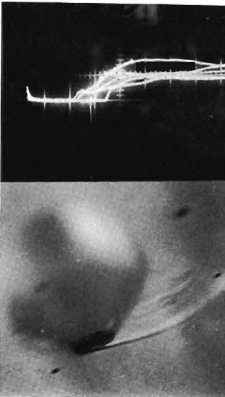
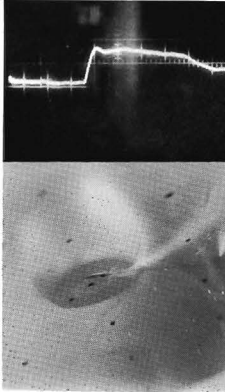


Figure 2.7.1

Photographs of bubbles
and simultaneous temperature recordings

Temperature drops and remains constant when thermocouple junction is inside bubble; it rises again after bubble release.

Large divisions on oscilloscope screen correspond to 5 K (vertically) and 10 ms (horizontally)

The heating current was taken from batteries in these experiments to prevent the occurrence of stray signals which could impede the determination of the small changes of the thermocouple voltage.

2.8. High-speed film camera

In our studies of burnout and bubble growth we used a Hitachi rotating prism high-speed camera, in most cases running at 4000 frames per second. Timing marks at 20 ms intervals were made on the edge of the films by a stroboscopic lamp with a flash duration of 1 μ s inside the camera synchronized to 50 Hz electricity mains frequency. The optical technique used for the observations made interpretation of the films quite simple. Kodak XX negative film was used.

The temperature drops on a photographic record of the oscilloscope screen, obtained simultaneously with the film, could be allocated to the various bubbles on the film by comparing the time intervals between the bubbles and the temperature drops. This technique was used for the final verification of the theory of bubble growth.

CHAPTER 3

BUBBLE GROWTH

3.1. The different phases of growth of a bubble

The growth of a spherical bubble has been analysed by Forster and Zuber²⁰ and by Plesset and Zwick²¹. In the latter paper a careful discussion of possible simplifications is given, and it is shown that the initial growth after nucleation will be followed by a period of growth controlled by heat transfer. In this section we will use a slightly different presentation to describe these consecutive phases of growth. The bubble radius will be denoted by r_b , which is initially equal to a nucleation-determined value r_c . Considering a spherical bubble we disregard the presence of the heating surface for the moment, in which case viscous effects can also be neglected. At nucleation we have

$$\left. \begin{aligned} r_b &= r_c \\ dr_b/dt &= 0 \end{aligned} \right\} t = 0 \quad (3.1.1)$$

where t is the time.

The superheat and excess pressure of the vapour in the bubble are constant at the values corresponding to equilibrium at the nucleation radius governed by equations (1.4.2) and (1.4.3). The excess pressure $p_v - p(\infty)$ will remain constant until the temperature at the bubble wall decreases.

Using the Rayleigh equation to obtain the dynamical pressure, opposing growth, exerted on a spherical bubble by the liquid surrounding it we have

$$\frac{p_v - p(\infty)}{\rho_l} = \frac{2\sigma}{\rho_l r_b} + r_b \frac{dr_b^2}{dt^2} + \frac{3}{2} \left(\frac{dr_b}{dt} \right)^2 \quad (3.1.2)$$

Upon multiplication by $r_b^2 dr_b/dt$ this equation can be integrated, leading to an expression for the bubble wall velocity, using also (1.4.2)

$$\left(\frac{dr_b}{dt}\right)^2 = \frac{2}{3} \frac{p_v - p(\infty)}{\rho_l} \left(1 - \frac{3}{2} \frac{r_c}{r_b} + \frac{1}{2} \frac{r_c^3}{r_b^3}\right). \quad (3.1.3)$$

The results of a numerical integration for a bubble, with initial radius $1.0001 r_c$ to start its growth, are shown in Figure 3.1.1.

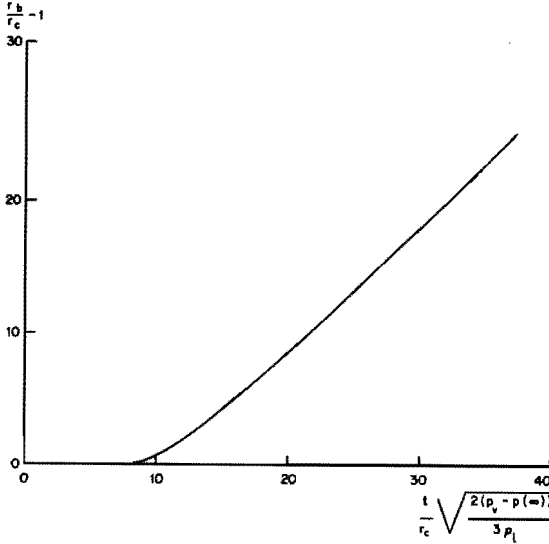


Figure 3.1.1

Calculated initial growth of spherical bubble
in dimensionless representation

With increasing bubble radius the velocity will approach a constant value. This growth rate cannot be sustained, however, During growth with r_b proportional to t , evaporation will withdraw heat from a skin of increasing thickness, of the order of $(a_l t)^{\frac{1}{2}}$, around the bubble, the skin volume increasing proportionally with $t^{5/2}$. a_l is the heat diffusivity of the liquid. The heat withdrawn is converted to latent heat present in the bubble, in an amount proportional to t^3 . The temperature around the bubble must therefore decrease, decreasing the vapour pressure and thereby the rate

of growth. Ultimately the temperature of the vapour in the bubble will approach the saturation value T_0 , the bubble growth rate tending asymptotically to the value which is determined by heat conduction to the bubble.

More quantitative results about the successive phases of growth of a spherical bubble surrounded by liquid were obtained in a numerical study by Waldman and Houghton²². A very concisely formulated analysis of the rapid heat transfer-controlled growth of a spherical bubble was given by Birkhoff et al.²³.

We have studied this phase of growth controlled by heat transfer for a bubble at the heating surface. It is usually indicated as the phase of rapid growth because the bubble Reynolds number then attains its maximum value.

3.2. The microlayer under a bubble

The growth of bubbles at a heating surface differs from that of bubbles surrounded by liquid. In this section the literature on growth at a heating surface is discussed together with our initial results.

The study of bubble growth has received renewed attention since Moore and Mesler²⁴ recorded rapid temperature drops with small thermocouples inserted into a metal strip heating surface near or at a site generating bubbles. On the basis of their findings they postulated the presence of a rapidly evaporating thin liquid layer under a bubble growing at a plane heating surface. Although their detailed interpretation of the observed surface cooling was not quite correct, other explanations also being possible as discussed by Van Stralen²⁵, later work showed that the microlayer concept was correct for bubbles generated at a plane heating surface. Indirect support for the microlayer hypothesis was obtained by Rogers and Mesler²⁶. Synchronously with the temperature recordings they made photographs of the associated bubbles, a technique which we copied for temperature measurements in the vicinity of and inside a bubble, as described in Section 2.7. In this way they showed that the alternative explanation for the rapid temperature drop - inflow of cold liquid after bubble departure - was not tenable. Hospeti and Mesler²⁷

further tried to measure microlayer thicknesses by determination of the amount of scale deposited around an active site by a known large number of bubbles. Techniques similar to Moore and Mesler's²⁴ were employed by Bonnet, Macke and Morin²⁸ and by Madsen²⁷. Their results are also discussed by Van Stralen²³.

Sharp³⁰ was the first to observe the microlayer directly on a transparent heating surface, heated by means of a hot gas jet, by applying optical interference methods. He sometimes noticed the presence of a dry area at its centre. His thickness measurements cannot be compared with our results because they are not directly related to bubble size and growth rate, which, as we shall see, is necessary. Note that no reference is made to a hemispherical shape of the bubble in this paper. In this early work a uniform initial microlayer thickness was tacitly assumed, and the discussion centred around the way in which it evaporated. Although this evaporation will certainly have important consequences for bubble growth, a theory incorporating this effect did not exist and studies of bubble growth rates at the heating surface still had to be analysed using the results for the rapid growth of spherical bubbles surrounded by liquid, as in the paper by Cole and Shulman³¹.

In our experiments on bubbles growing at the heating surface in n-heptane at low pressure the microlayer was clearly visible. Our initial results were as follows.

A growing bubble has a hemispherical shape. Its radius r_b increases with time t according to the relation $r_b = kt^{\frac{1}{2}}$, where k is the growth constant. Under the bubble the microlayer covers the heated surface. Near the centre of the bubble the heated surface is dry. The dry area grows together with the bubble, which indicates that evaporation of the liquid film occurs.

We found a model for this growth process which served as a useful first step on the way to its complete description. Some aspects of the model are unrealistic, but it is simple and illustrative. Assume the hemispherical bubble to be growing on the solid surface under the influence of the evaporation at the liquid film only, for which the necessary heat is withdrawn from the solid by a transient cooling process. Actually evap-

poration at the hemispherical surface contributes to the growth rate as will be discussed later, but this is of no importance in the present argument. Using cylindrical polar coordinates, indicated by a tilde, the heat conduction is assumed to occur in the \tilde{z} -direction only, which is perpendicular to the surface. The constant electrical heat input is neglected, just as the influence of the liquid film on the heat conduction to the bubble, its role being restricted to the conversion into vapour of the heat supplied to the bubble.

When the solid is initially superheated at a temperature T_1 , the supply of heat to the bubble at the position $\tilde{r} = \tilde{r}_1$ at the surface of the solid ($\tilde{r} = 0$ is the centre of the bubble) begins at the moment $t = t_1$, when the bubble boundary passes this position and the saturation temperature T_0 of the vapour in the bubble is imposed. \tilde{r}_1 and t_1 are connected by the growth relation for the bubble $\tilde{r} = r_b(t)$, which determines the position at the surface of the solid of the hemispherical bubble wall, hence $\tilde{r}_1 = r_b(t_1)$. The heat flux Φ at the surface of the solid at that position is

$$\Phi = \pi^{-\frac{1}{2}} (\lambda_s \rho_s c_s)^{\frac{1}{2}} \frac{T_1 - T_0}{(t - t_1)^{\frac{1}{2}}} \quad (3.2.1)$$

which is converted into a volumetric flux Ω of vapour

$$\Omega = \pi^{-\frac{1}{2}} \frac{(\lambda_s \rho_s c_s)^{\frac{1}{2}} (T_1 - T_0)}{\rho_v L} \frac{1}{(t - t_1)^{\frac{1}{2}}} \quad (3.2.2)$$

λ_s , ρ_s and c_s are the heat conductivity, density and specific heat of the solid, respectively. Under the conditions of our experiments the constant electrical heat input can be neglected in comparison with the flux Φ .

The balance equation for the vapour is obtained by equating the total vapour production over the surface under the bubble to the rate of increase of the bubble volume at a chosen moment. The result is

$$2\pi r_b^2 \frac{dr_b}{dt} = \frac{\pi^{-\frac{1}{2}} (\lambda_s \rho_s c_s)^{\frac{1}{2}}}{\rho_v L} \int_0^{r_b} \frac{T_1 - T_0}{(t - t_1)^{\frac{1}{2}}} 2\pi \tilde{r}_1 d\tilde{r}_1 \quad (3.2.3)$$

The growth relation $r_b = kt^{\frac{1}{2}}$ satisfies this equation, as can be seen when we carry out the substitutions $t = r_b^2/k^2$ and $t_1 = \tilde{r}_1^2/k^2$.

The value for the growth constant k is then

$$k = 2\pi^{-\frac{1}{2}} \frac{(\lambda_s \rho_s c_s)^{\frac{1}{2}}}{\rho_v L} (T_1 - T_0) \quad (3.2.4)$$

When the model is considered again, we realize that the distance of penetration of the transient cooling in the z -direction into the solid may well be small in the short time interval necessary for a bubble to grow. If the thickness of the liquid film were larger, it would be more appropriate to use the thermal constants for the liquid instead of those for the solid. In that case we would have:

$$k = 2\pi^{-\frac{1}{2}} \frac{(\lambda_l \rho_l c_l)^{\frac{1}{2}}}{\rho_v L} (T_1 - T_0) \quad (3.2.5)$$

Note that the way in which the liquid film is treated is unrealistic in both cases. In the first, we make the formal mistake of neglecting its influence on the heat conduction, in the second we discard our observation that the film evaporates to dryness. To determine whether liquid or solid thermal constants should be used we compared bubble growth on pyrex glass and perspex, transparent materials with different values of the contact coefficient $(\lambda\rho c)^{\frac{1}{2}}$. The following conclusions resulted (cf. Tables 5.2.1 and 5.2.2):

- (1) Bubble growth is hardly affected by the solid thermal constants.
- (2) The radius of the dry area under the bubble increases markedly with increasing ratio of the contact coefficients, $(\lambda_s \rho_s c_s / \lambda_l \rho_l c_l)^{\frac{1}{2}}$.

The first conclusion has also been drawn in a recent paper by Sernas and Hooper³² from experiments with a plane heating surface. They did not use different solids, however, but compared equations (3.2.4) and (3.2.5) with observed growth rates. We feel that this procedure cannot be considered as entirely conclusive because of the varying contribution to the growth rate of evaporation at the hemispherical surface, which is discussed in Chapter 5. Their experiment did not allow observations relating to the second conclusion.

As both bubble growth and dry area radius depend directly on microlayer evaporation, the two conclusions confronted us with a contradiction, which

led us to the description of the bubble growth process presented in Chapter 4. An essential element revealed by the theory is that the initial microlayer thickness is not uniform.

Since then a number of papers have appeared which pointed to this fact. They all consider a hemispherical bubble shape. Torikai³³ and Torikai and Yamazaki³⁴ studied bubble growth using an experimental technique which is practically the same as ours. Instead of glass they used a liquid prism, and whereas we employed diffuse light coming from the side of the boiling liquid, they used a beam incident on another face of their prism which was reflected by the heating surface. This technique is slightly disadvantageous in that well-aligned optical systems are required. On the other hand the liquid is not disturbed by the presence of a lamp. In both papers the basis of their discussion of microlayer and bubble growth is a force balance on a volume element of the microlayer. As, however, the excess pressure in the bubble can be regarded as a hydrostatic pressure acting on the entire microlayer, the force balance which they used is incomplete.

A major step forward resulted from the work done by Cooper and Lloyd³⁵. They used a glass heating surface, heated by radiation, as the carrier of a minuscule array of semiconductor resistance thermometers applied to the surface by vacuum evaporation. In contradistinction with our experiments no observations were made through the surface. A current pulse through one resistance generated a bubble, the other resistances were used to record temperature changes. With some auxiliary assumptions concerning the heat conduction process these temperatures were integrated with respect to time and used to calculate the local original microlayer thickness in two different ways. The values obtained compare favourably with those derived from our experiments.

In an appended paper Cooper³⁶ used these findings to set up a bubble growth theory which was the first one incorporating microlayer evaporation. The contents of these two papers cover many aspects of the problem of bubble growth. In Section 5.3 they will be compared with the results on bubble growth presented in Chapters 4 and 5, which will be seen to offer a more satisfactory description of various aspects of the problem.

Essentially the same experimental technique as that of Cooper and Lloyd³⁵ was used by McSweeney³⁷. His analysis makes use of numerical calculations at an early stage and is further equivalent to that of Cooper and Lloyd³⁵. We mention two more papers here. The first is a calculation of microlayer thickness by Olander and Watts³⁸ which will be discussed later, in the second Jawurek³⁹ describes a promising interference experiment to measure the thickness of the microlayer. So far only preliminary information has been obtained, probably related to the time interval in which bubble release starts.

CHAPTER 4

THEORY OF RAPID BUBBLE GROWTH AT A LIQUID-SOLID INTERFACE

4.1. Statement of the problem

As we have seen, vapour bubbles in a boiling liquid are formed by heterogeneous nucleation in cavities at the heating surface. To understand what happens after nucleation the growth of a vapour bubble at a liquid-solid interface must be studied.

From the study of growth of spherical bubbles by Waldman and Houghton²² it is known that various phases can be distinguished in the growth history. We focus our attention on the phase of rapid growth, when the growth rate is controlled by the rate of heat transfer to the bubble. Birkhoff et al.²³ have given a theoretical description for a spherical bubble, but this situation is not representative of nucleate boiling. The presence of the solid-liquid interface imposes boundary conditions which lead to more complicated temperature and flow fields, introducing viscous effects which cause the formation of the microlayer.

We carry out the analysis for the case of uniform initial superheat of liquid and solid. The dimensions of the solid and liquid media are taken sufficiently large to regard these as semi-infinite bodies. Although not being a necessary simplification, the initial superheat is assumed to be so small that the physical constants of liquid and solid may be considered to be independent of temperature. A general consideration of the problem structure in Section 4.2 will reveal information about the solution which simplifies further analysis. In Sections 4.3, 4.4 and 4.5 the processes of flow, heat conduction and evaporation in the liquid and in the boundary layer at the solid surface will be studied separately.

4.2. General aspects of rapid bubble growth

Consider the growth of a vapour bubble at the plane interface between a liquid and a solid medium in the absence of surface tension and gravity. Spherical polar coordinates r, ϑ, φ with the origin at the interface will be used, of which only r and ϑ appear in the analysis because of the cylindrical symmetry around an axis perpendicular to the interface. The axis of symmetry is denoted by $\vartheta = 0$ in the liquid and by $\vartheta = \pi$ in the solid. The constant external pressure is again denoted by $p(\infty)$, the saturation temperature and density of the vapour at this pressure by T_0 and ρ_v , respectively. The initially uniform temperature of the liquid and the solid is T_1 , which is larger than T_0 .

In the present problem the stresses and pressure differences associated with the flow of the vapour inside the bubble will be unimportant when the velocity of the bubble boundary is small compared with that of sound waves in the vapour, since normally the density and the dynamic viscosity have much lower values for the vapour than for the liquid. Hence, we can state:

$$\frac{\rho_v}{\rho_l} \ll 1 \quad (4.2.1)$$

$$\frac{\rho_v \nu_v}{\rho_l \nu_l} \ll 1 \quad (4.2.2)$$

Here ν_l and ν_v are the kinematic viscosities of liquid and vapour, respectively. We therefore neglect the effects of the flow of the vapour and assume that the pressure p_v is uniform inside the bubble. p_v determines the temperature T_v and density ρ'_v of the vapour according to the saturation curve for the vapour-liquid equilibrium and the equation of state of the vapour.

The flow which is set up in the liquid around the growing bubble as a consequence of the increase in volume associated with evaporation must satisfy the Navier-Stokes and continuity equations.

$$\frac{\partial v_r}{\partial t} + v_r \frac{\partial v_r}{\partial r} + \frac{v_\vartheta}{r} \frac{\partial v_r}{\partial \vartheta} - \frac{v_\vartheta^2}{r} = - \frac{1}{r} \frac{\partial p_\ell}{\partial r} +$$

$$+ \nu_\ell \left\{ \frac{1}{r} \frac{\partial^2}{\partial r^2} (rv_r) + \frac{1}{r^2} \frac{\partial^2 v_r}{\partial \vartheta^2} + \frac{\cot \vartheta}{r^2} \frac{\partial v_r}{\partial \vartheta} - \frac{2}{r^2} \frac{\partial v_\vartheta}{\partial \vartheta} - \frac{2v_r}{r^2} - 2 \cot \vartheta \frac{v_\vartheta}{r^2} \right\}. \quad (4.2.3)$$

$$\frac{\partial v_\vartheta}{\partial t} + v_r \frac{\partial v_\vartheta}{\partial r} + \frac{v_\vartheta}{r} \frac{\partial v_\vartheta}{\partial \vartheta} + \frac{v_r v_\vartheta}{r} = - \frac{1}{r} \frac{\partial p_\ell}{\partial \vartheta} +$$

$$+ \nu_\ell \left\{ \frac{1}{r} \frac{\partial^2}{\partial r^2} (rv_\vartheta) + \frac{1}{r^2} \frac{\partial^2 v_\vartheta}{\partial \vartheta^2} + \frac{\cot \vartheta}{r^2} \frac{\partial v_\vartheta}{\partial \vartheta} + \frac{2}{r^2} \frac{\partial v_r}{\partial \vartheta} - \frac{v_\vartheta}{r^2 \sin^2 \vartheta} \right\}. \quad (4.2.4)$$

$$\frac{\partial v_r}{\partial r} + \frac{1}{r} \frac{\partial v_\vartheta}{\partial \vartheta} + \frac{2v_r}{r} + \cot \vartheta \frac{v_\vartheta}{r} = 0. \quad (4.2.5)$$

v_r and v_ϑ are the components of the liquid velocity.

The heat conduction in the liquid and in the solid is governed by the diffusion equations

$$\frac{\partial T_\ell}{\partial t} + v_r \frac{\partial T_\ell}{\partial r} + \frac{v_\vartheta}{r} \frac{\partial T_\ell}{\partial \vartheta} = a_\ell \left\{ \frac{1}{r} \frac{\partial^2}{\partial r^2} (rT_\ell) + \frac{1}{r^2} \frac{\partial^2 T_\ell}{\partial \vartheta^2} + \frac{\cot \vartheta}{r^2} \frac{\partial T_\ell}{\partial \vartheta} \right\}, \quad (4.2.6)$$

and

$$\frac{\partial T_s}{\partial t} = a_s \left\{ \frac{1}{r} \frac{\partial^2}{\partial r^2} (rT_s) + \frac{1}{r^2} \frac{\partial^2 T_s}{\partial \vartheta^2} + \frac{\cot \vartheta}{r^2} \frac{\partial T_s}{\partial \vartheta} \right\}. \quad (4.2.7)$$

Here T_ℓ and T_s are the temperatures of the liquid and the solid, respectively, and a_ℓ and a_s their heat diffusivities.

Let the vapour-liquid interface S of the bubble be described by

$$r = r_b^*(t, \vartheta). \quad (4.2.8)$$

If at some moment the vapour is in direct contact with the solid, this will occur over a circular area owing to the symmetry. We denote the radius of this area by r_d

$$r_d = r_b^*(t, \frac{\pi}{2}). \quad (4.2.9)$$

On the solid surface outside this area the liquid velocity must be zero, both perpendicular and parallel to the solid surface,

$$v_r = 0 \quad \text{at} \quad \vartheta = \frac{\pi}{2}, \quad r \geq r_d, \quad (4.2.10)$$

$$v_\vartheta = 0 \quad \text{at} \quad \vartheta = \frac{\pi}{2}, \quad r \geq r_d. \quad (4.2.11)$$

Further the temperature and the heat flux perpendicular to the surface must be continuous there:

$$T_\ell = T_s \quad \text{at} \quad \vartheta = \frac{\pi}{2}, \quad r \geq r_d, \quad (4.2.12)$$

$$\lambda_\ell \frac{\partial T_\ell}{\partial \vartheta} = \lambda_s \frac{\partial T_s}{\partial \vartheta} \quad \text{at} \quad \vartheta = \frac{\pi}{2}, \quad r \geq r_d. \quad (4.2.13)$$

where λ_ℓ and λ_s are the heat conductivities of the liquid and the solid, respectively.

The heat conduction to the bubble in the area where the solid is in direct contact with the vapour in the bubble is of little importance as no change of phase is involved. It will be neglected. With

$$\frac{\lambda_v}{\lambda_s} \ll 1 \quad (4.2.14)$$

this leads to the condition

$$\frac{\partial T_s}{\partial \vartheta} = 0 \quad \text{at} \quad \vartheta = \frac{\pi}{2}, \quad r < r_d. \quad (4.2.15)$$

At the vapour-liquid interface of the bubble the liquid temperature is equal to the vapour temperature,

$$T_\ell = T_v \quad \text{at} \quad S. \quad (4.2.16)$$

Considering a surface element dS at some point on the bubble surface, we take ψ for the angle between the outward normal to the surface element and the radius vector at that point. ψ is determined by the relation

$$\tan \psi = - \frac{1}{r_b^*} \left(\frac{\partial r_b^*}{\partial \vartheta} \right)_t = \text{const.} \quad (4.2.17)$$

A balance of forces at the surface element, neglecting the effects of vapour flow, leads to the conditions

$$p_v \cos \psi = \left\{ p_\ell - 2\rho_\ell \nu_\ell \frac{\partial v_r}{\partial r} \right\} \cos \psi - \rho_\ell \nu_\ell \left\{ \frac{1}{r} \frac{\partial v_r}{\partial \vartheta} + \frac{\partial v_\vartheta}{\partial r} - \frac{v_\vartheta}{r} \right\} \sin \psi, \quad \text{at S, (4.2.18)}$$

and

$$p_v \sin \psi = \left\{ p_\ell - 2\rho_\ell \nu_\ell \left(\frac{1}{r} \frac{\partial v_\vartheta}{\partial \vartheta} + \frac{v_r}{r} \right) \right\} \sin \psi - \\ - \rho_\ell \nu_\ell \left\{ \frac{1}{r} \frac{\partial v_r}{\partial \vartheta} + \frac{\partial v_\vartheta}{\partial r} - \frac{v_\vartheta}{r} \right\} \cos \psi, \quad \text{at S. (4.2.19)}$$

See Landau and Lifshitz⁴⁰. The heat conducted to the bubble surface can be equated to the loss of liquid due to evaporation, which quantity in turn determines the local mass flux Ψ of vapour into the bubble.

$$\lambda_\ell \left(\frac{\partial T_\ell}{\partial r} \cos \psi + \frac{1}{r} \frac{\partial T_\ell}{\partial \vartheta} \sin \psi \right) =$$

$$L\rho_\ell \left\{ \left(\frac{\partial r_b}{\partial t} \right)_{\vartheta = \text{const}} \cos \psi - (v_r \cos \psi + v_\vartheta \sin \psi) \right\} = L\Psi, \quad \text{at S. (4.2.20)}$$

The total vapour flux into the bubble is equal to the rate of increase of the total mass inside the bubble,

$$\int_S \Psi \, dS = \frac{d(\rho_v V)}{dt}, \quad (4.2.21)$$

where V is the volume of the bubble.

The conditions at infinity can be stated as follows.

$$\begin{aligned} T_s &\rightarrow T_1 && \text{when } r \rightarrow \infty, \quad \frac{\pi}{2} \leq \vartheta \leq \pi \\ T_\ell &\rightarrow T_1 && \text{when } r \rightarrow \infty, \quad 0 \leq \vartheta \leq \frac{\pi}{2} \\ p_\ell &\rightarrow p(\infty) && \text{when } r \rightarrow \infty, \quad 0 \leq \vartheta \leq \frac{\pi}{2} \\ v_r &\rightarrow 0 && \text{when } r \rightarrow \infty, \quad 0 \leq \vartheta \leq \frac{\pi}{2} \\ v_\vartheta &\rightarrow 0 && \text{when } r \rightarrow \infty, \quad 0 \leq \vartheta \leq \frac{\pi}{2} \end{aligned} \quad (4.2.22)$$

In view of symmetry and the required absence of singularities the solution must further satisfy the following conditions

$$\begin{aligned}
 \left(\frac{\partial r_b^*}{\partial \vartheta}\right)_{t = \text{const}} &= 0 & \text{at } \vartheta &= 0 \\
 \frac{\partial T_s}{\partial \vartheta} &= 0 & \text{at } \vartheta &= \pi \\
 \frac{\partial T_\ell}{\partial \vartheta} &= 0 & \text{at } \vartheta &= 0 & r \geq r_b^* \\
 \frac{\partial v_r}{\partial \vartheta} &= 0 & \text{at } \vartheta &= 0 & r \geq r_b^* \\
 v_\vartheta &= 0 & \text{at } \vartheta &= 0 & r \geq r_b^* \\
 \frac{\partial p_\ell}{\partial \vartheta} &= 0 & \text{at } \vartheta &= 0 & r \geq r_b^* \\
 \frac{\partial T_s}{\partial r} &= 0 & \text{at } r &= 0 & \frac{\pi}{2} < \vartheta \leq \pi
 \end{aligned} \tag{4.2.23}$$

Apart from initial conditions which remain to be specified, the equations and conditions given above define the problem.

An important simplification arises when we restrict ourselves to the phase of growth during which the driving pressure difference $p_v - p(\infty)$ needed to enlarge the bubble satisfies the conditions

$$\frac{p_v - p(\infty)}{(\frac{dp_v}{dT_v})(T_1 - T_0)} \ll 1 \quad , \tag{4.2.24}$$

and

$$\frac{p_v - p(\infty)}{p(\infty)} \ll 1 \quad . \tag{4.2.25}$$

Here dp_v/dT_v denotes the slope of the saturation curve at (p_v, T_v) . As both (p_v, T_v) and $(p(\infty), T_0)$ are points on the saturation curve, condition (4.2.24) implies that we restrict our attention to the case when the change in the vapour temperature caused by the dynamic excess pressure is negligible compared with the initial superheat:

$$\frac{T_v - T_0}{T_1 - T_0} \ll 1 \quad , \quad (4.2.26)$$

which shows that condition (4.2.17) can be replaced by the condition

$$T_\ell = T_0 \quad \text{at} \quad S \quad . \quad (4.2.27)$$

Similarly, by using the ideal-gas law as an approximation to the equation of state of the vapour, we can easily see that condition (4.2.25) is equivalent to

$$\frac{\rho'_v - \rho_v}{\rho_v} \ll 1 \quad , \quad (4.2.28)$$

which shows that the vapour density ρ'_v does not differ notably from the saturation density ρ_v at $p(\infty)$. Condition (4.2.21) can therefore be replaced by

$$\int_S \Psi dS = \rho_v \frac{dV}{dt} \quad . \quad (4.2.29)$$

The general properties of the solution of the problem simplified in this manner can now be determined.

We shall verify that the problem defined by expressions (4.2.3) to (4.2.15), (4.2.17) to (4.2.20), (4.2.22), (4.2.23), (4.2.27) and (4.2.29) has a solution which only depends on two independent dimensionless variables α and ϑ , where α is defined as

$$\alpha = \frac{r}{kt^{\frac{1}{2}}} \quad . \quad (4.2.30)$$

k is a constant. This can only be the case if all equations and conditions of the problem can be transformed to expressions containing only the variables α and ϑ , functions of these variables and derivatives with respect to them, and if the bubble has a surface of fixed shape:

$$\alpha = \alpha_b(\vartheta) \quad . \quad (4.2.31)$$

Note that according to this solution the surface of the bubble will be given by

$$r = kt^{\frac{1}{2}} \alpha_b(\vartheta) \quad (4.2.32)$$

in the t, r, ϑ system. Owing to the presence of the unspecified constant k in (4.2.32) the dimensionless shape factor $\alpha_b(\vartheta)$ can be normalized in such a way that

$$\alpha_b(0) = 1 \quad (4.2.33)$$

The constant k can be called the growth constant of the bubble as it determines growth in the direction $\vartheta = 0$ in view of (4.2.33).

We introduce the following dimensionless quantities,

$$\theta_\ell = \frac{T_\ell - T_0}{T_1 - T_0} \quad , \quad (4.2.34)$$

$$\theta_s = \frac{T_s - T_0}{T_1 - T_0} \quad , \quad (4.2.35)$$

$$w_r = \frac{v_r t^{\frac{1}{2}}}{k} \quad , \quad (4.2.36)$$

$$w_\vartheta = \frac{v_\vartheta t^{\frac{1}{2}}}{k} \quad , \quad (4.2.37)$$

$$Q_\ell = \frac{\{p_\ell - p(\infty)\}t}{\rho_\ell k^2} \quad , \quad (4.2.38)$$

$$Q_v = \frac{\{p_v - p(\infty)\}t}{\rho_\ell k^2} \quad . \quad (4.2.39)$$

When we consider (4.2.34) to (4.2.39) as dependent variables which are functions of α and ϑ , it is found that transformation to the newly defined independent and these dependent variables removes the variables r and t from all equations and conditions. This confirms the original assumption that the problem has a solution which depends on α and ϑ only. A solution of this type is usually called a self-similar solution.

Note that Q_v is a constant because p_v is not a function of position.

Only the following initial conditions for the original problem are compatible with the self-similar solution:

$$T_{\ell} = T_s = T_1 \quad \text{at} \quad t = 0 \quad (4.2.40)$$

$$r_b^* = 0 \quad \text{at} \quad t = 0 \quad (4.2.41)$$

The first condition is that of initial uniform superheat which was assumed at the outset. But the simplifying conditions (4.2.24) and (4.2.25) and the initial condition (4.2.41) are not satisfied during the initial growth of an actual bubble. The bubble growth rate tends asymptotically to the rate predicted by the self-similar solution only after the phase of initial growth.

Upon inspection of conditions (4.2.1), (4.2.20) and (4.2.29) at $\vartheta = 0$, noting that $\psi = 0$ in view of (4.2.23) and (4.2.27), we see that

$$\left(\frac{\partial r_b^*}{\partial t}\right)_{\vartheta=0} - v_r(t, r_b^*, 0) \ll \left(\frac{\partial r_b^*}{\partial t}\right)_{\vartheta=0} \quad (4.2.42)$$

This result is used to determine the Reynolds number for the flow around the growing bubble which is defined as

$$R = \frac{v_r(t, r_b^*, 0) r_b^*(t, 0)}{\nu_{\ell}} \quad (4.2.43)$$

With (4.2.42), using also (4.2.32) and (4.2.33), we obtain the value

$$R = \frac{k^2}{2 \nu_{\ell}} \quad (4.2.44)$$

which is independent of time.

With the use of (4.2.41) the restrictions as to the validity of the self-similar solution imposed by the simplifying conditions (4.2.24) and (4.2.25) can be formulated as follows:

$$Q_v \frac{T_0 \rho_{\ell} k^2}{(T_1 - T_0) \rho_v L t} \ll 1 \quad (4.2.45)$$

and

$$Q_v \frac{\rho_l k^2}{p^{(\infty)} t} \ll 1 \quad , \quad (4.2.46)$$

where dp_v/dT has been replaced by $\rho_v L/T_0$ with the help of the Clausius-Clapeyron equation, taking into account (4.2.1). From these results it can now be seen that the self-similar solution described in the foregoing does not apply to the initial phase of bubble growth.

Effects of surface tension and gravity can formally be incorporated in the theory, but the presence of the corresponding terms in the various expressions makes it impossible to remove the time variable from the problem. Therefore the self-similar solution is only applicable when these effects are small enough not to affect the pressure distribution in the liquid at the bubble surface. This will be the case if both the pressure difference across a distance of the order of the bubble dimensions due to gravity and that across the bubble surface due to surface tension are small compared with the dynamic excess pressure at the bubble. When σ is the surface tension and g the acceleration of gravity we see that the first quantity is $\frac{1}{2} \rho_l g k t^{\frac{1}{2}}$ and the second $2\sigma/kt^{\frac{1}{2}}$, as both the dimensions of the bubble and the radii of curvature at each point are proportional to $kt^{\frac{1}{2}}$ according to (4.2.32). Using again (4.2.39) we see that the time interval during which the self-similar solution is applicable is further restricted by the following conditions:

$$\frac{1}{2} \frac{g t^{3/2}}{Q_v k} \ll 1 \quad , \quad \text{and} \quad (4.2.47)$$

$$\frac{2}{Q_v} \frac{\sigma t^{\frac{1}{2}}}{\rho_l k^3} \ll 1 \quad . \quad (4.2.48)$$

Even with the general knowledge of the existence of the self-similar solution the problem remains a very complicated one, except in the case of rapid growth when the viscous effects are confined to a thin layer of liquid near the surface of the solid. The problem then falls apart into two related problems, one concerning the main stream region and the other the region near the solid-liquid boundary, which can be studied separately. We shall turn our attention to this situation in the following sections. Once the solution has been obtained, the values of the numeri-

cal constant in equations (4.2.45) to (4.2.48) can be determined. Integration of (4.3.4) yields $Q_v = \frac{1}{8}$.

We assume in what follows that these conditions are satisfied. Therefore, as has been mentioned already, the theory applies to a certain phase of the bubble growth process only. When the pressure effects corresponding to the effects of superheat, acceleration, gravity and surface tension are plotted against the bubble radius, as is done in Figure 4.2.1 for two values of $T_1 - T_0$, the phase of growth described can easily be identified.

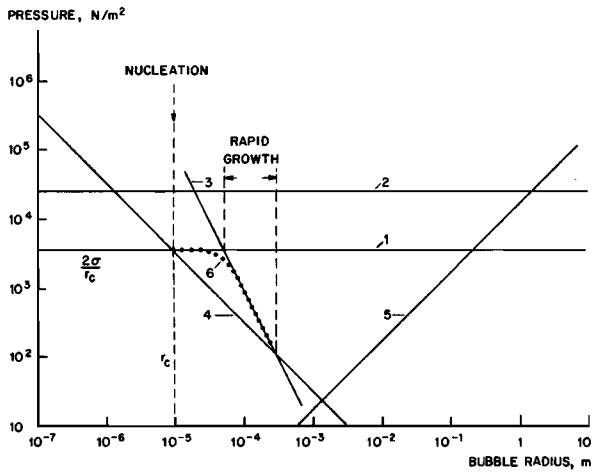
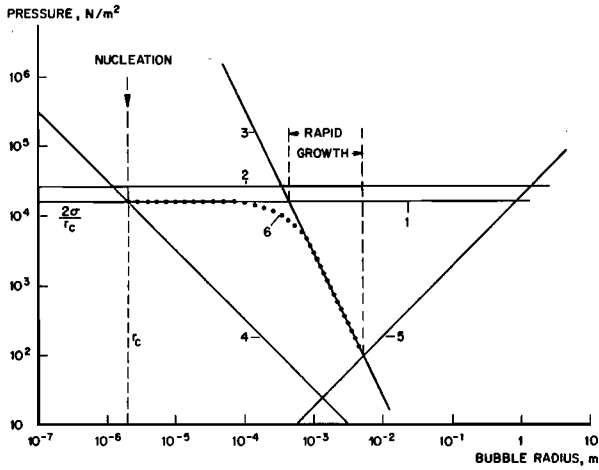


Figure 4.2.1

Pressure effects which determine the growth history of a bubble

Calculated for hypothetical bubbles growing in n-heptane at a pressure of 24.6 kN/m² at uniform superheats of 17.5 K and 4 K, respectively,

Dynamical pressure is for growth following $r_b = kt^{\frac{2}{3}}$

1 = maximum excess pressure for given superheat $\Delta p \approx \rho_v L \Delta T / T$

2 = ambient pressure $p(\infty)$

3 = dynamical excess pressure $\Delta p = \rho_l k^4 / (8r_b^2)$

4 = surface tension excess pressure $\Delta p = 2\sigma/r_b$

5 = pressure difference across bubble due to gravity $\Delta p = \frac{1}{2} \rho_l g r_b$

6 = actual excess pressure in growing bubble $p_v - p(\infty)$ (qualitatively)

4.3. The flow field and the formation of the microlayer

When the effects of surface tension and gravity are negligible, the Reynolds number

$$R = \frac{k^2}{2 \nu_l} \quad (4.2.44)$$

characterizes the flow field around a growing bubble. The Reynolds number associated with a rapidly growing bubble has a large value, of the order of 3000 in our experiments. Consequently, the flow field around such a bubble resembles non-viscous flow except in a thin layer on the solid surface where the no-slip boundary condition has to be satisfied. The main flow will be uniformly radial, as for non-viscous flow there is no preferred direction in this situation.

These properties of the flow field determine the shape of the bubble, which grows as a hemisphere with a thin layer of liquid left on the surface of the solid underneath. A qualitative sketch of the shape of the bubble is given in Figure 4.3.1. In view of the foregoing, it is clear

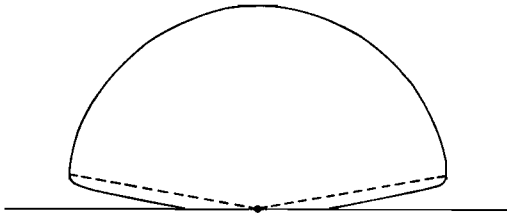


Figure 4.3.1

Shape of the growing bubble

Broken line indicates microlayer thickness at each point before being decreased by evaporation

that the hemisphere with radius r_b will grow according to the relation

$$r_b = kt^{\frac{1}{2}} \quad (4.3.1)$$

With the condition

$$v_r = \frac{dr_b}{dt} \quad \text{at } r = r_b \quad , \quad (4.3.2)$$

in view of (4.2.41), the spherical flow field can be described by

$$v_r = \frac{k^3 t^{\frac{1}{2}}}{2r^2} \quad , \quad r \geq r_b \quad , \quad (4.3.3)$$

while the pressure gradient is found from

$$-\frac{1}{\rho_l} \frac{\partial p_l}{\partial r} = \frac{dv_r}{dt} = \frac{\partial v_r}{\partial t} + v_r \frac{\partial v_r}{\partial r} = \frac{k^3}{2r^2 t^{\frac{1}{2}}} \left(\frac{1}{2} - \frac{r_b^3}{r^3} \right) \quad . \quad (4.3.4)$$

In the early phase of growth controlled by the maximum dynamical pressure in the bubble the liquid is accelerated everywhere outside the bubble. Flow reversal associated with deceleration (see Landau and Lifshitz⁴¹) cannot occur therefore and a boundary layer type of flow must have developed during this growth phase. If flow reversal were to occur later, when growth is retarded to the rate corresponding to (4.3.1), it would originate from separation of the boundary layer, because any deceleration is enhanced there by the viscous forces. But from (4.3.4) it can be seen that during growth according to (4.3.1) the flow is accelerated in the region

$$\frac{r^3}{r_b^3} > 2 \quad (\alpha^3 > 2) \quad , \quad (4.3.5)$$

and although the liquid is subject to an adverse pressure gradient in the region

$$1 < \frac{r^3}{r_b^3} < 2 \quad (1 < \alpha^3 < 2) \quad (4.3.6)$$

separation of the boundary layer will not occur here either, as will be shown in Section 4.4.

As the presence of the microlayer under the bubble is a direct consequence of the viscosity of the liquid, its thickness is in first instance

determined by the thickness of the boundary layer on the solid surface, to be modified later by evaporation.

In the previous section we have seen that the bubble retains its shape during growth, so the thickness $h_0(r_b)$ of the liquid layer at the point where it is formed by the proceeding hemispherical bubble boundary must be proportional to the radius of the bubble,

$$h_0(r_b) = C_1 r_b \quad . \quad (4.3.7)$$

The dimensionless thickness of the boundary layer outside the bubble is proportional to $R^{-\frac{1}{2}}$, so we can write

$$h_0(r_b) = r_b Z_b R^{-\frac{1}{2}} \quad , \quad (4.3.8)$$

where Z_b denotes a general dimensionless constant for a flow field of this type.

If we define the original thickness of the liquid layer under the bubble at a certain point as the thickness the layer had when it was formed, we have

$$h_0(r) = r Z_b R^{-\frac{1}{2}} \quad , \quad r \leq r_b \quad . \quad (4.3.9)$$

This expression will be used to describe evaporation at the microlayer surface in Section 4.5.

4.4. The boundary layer problem

To establish that growth of a bubble with a microlayer is possible the boundary layer must be studied in detail. In this section we will show that separation will not occur in the region outside the bubble and calculate the value of the constant Z_b . We proceed with the analysis of the growth process on the basis of (4.3.9) in Section 4.5.

The boundary layer problem is a time-dependent one. We again use cylindrical polar coordinates \tilde{r} and \tilde{z} , the positive \tilde{z} -axis corresponding to $\vartheta = 0$ and consider the region outside the bubble. The components of the liquid velocity are \tilde{v}_r and \tilde{v}_z . The continuity equation

$$\frac{\partial \tilde{v}_r}{\partial \tilde{r}} + \frac{\tilde{v}_r}{\tilde{r}} + \frac{\partial \tilde{v}_z}{\partial \tilde{z}} = 0 \quad , \quad (4.4.1)$$

is identically satisfied when a stream function φ_b is introduced such that

$$\tilde{v}_r = \frac{1}{\tilde{r}} \frac{\partial \varphi_b}{\partial \tilde{z}} \quad , \quad (4.4.2)$$

and

$$\tilde{v}_z = - \frac{1}{\tilde{r}} \frac{\partial \varphi_b}{\partial \tilde{r}} \quad . \quad (4.4.3)$$

For large values of R the boundary layer is confined to a narrow region near the solid where

$$\tilde{z} = O(R^{-\frac{1}{2}}) \quad . \quad (4.4.4)$$

Order of magnitude considerations show that the pressure distribution in the boundary layer is that of the main stream region given by (4.3.4), r being replaced by \tilde{r} in view of (4.4.4). The radial component of the Navier-Stokes equations then takes the form

$$\begin{aligned} & \frac{1}{\tilde{r}} \frac{\partial^2 \varphi_b}{\partial \tilde{z} \partial t} - \frac{1}{\tilde{r}^3} \left(\frac{\partial \varphi_b}{\partial \tilde{z}} \right)^2 + \frac{1}{\tilde{r}^2} \frac{\partial \varphi_b}{\partial \tilde{z}} \frac{\partial^2 \varphi_b}{\partial \tilde{z} \partial \tilde{r}} - \frac{1}{\tilde{r}^2} \frac{\partial \varphi_b}{\partial \tilde{r}} \frac{\partial^2 \varphi_b}{\partial \tilde{z}^2} = \\ & = \frac{k^3}{2\tilde{r}^2 t^{\frac{1}{2}}} \left(\frac{1}{2} - \frac{k^3 t^{3/2}}{\tilde{r}^3} \right) + \nu \left[\frac{\partial^2}{\partial \tilde{r}^2} \left(\frac{1}{\tilde{r}} \frac{\partial \varphi_b}{\partial \tilde{z}} \right) + \frac{1}{\tilde{r}} \frac{\partial^3 \varphi_b}{\partial \tilde{z}^3} + \frac{1}{\tilde{r}} \frac{\partial}{\partial \tilde{r}} \left(\frac{1}{\tilde{r}} \frac{\partial \varphi_b}{\partial \tilde{z}} \right) - \frac{1}{\tilde{r}^3} \frac{\partial \varphi_b}{\partial \tilde{z}} \right]. \quad (4.4.5) \end{aligned}$$

The relative order of magnitude of the terms, after the brackets have been removed, is 1, 1, 1, 1, 1, 1, R^{-1} , 1, R^{-1} , R^{-1} . The terms of order R^{-1} will be neglected.

The boundary conditions are

$$\left. \begin{aligned} \tilde{v}_r &= 0 \\ \tilde{v}_z &= 0 \end{aligned} \right\} \text{ at } \tilde{z} = 0 \quad , \quad (4.4.6)$$

and

$$\tilde{v}_r \rightarrow \frac{k^3 t^{\frac{1}{2}}}{2\tilde{r}^2} \text{ at the top of the boundary layer,} \quad (4.4.7)$$

in view of (4.3.3).

Using the self-similarity of the solution we introduce new independent variables

$$\tilde{\alpha} = \frac{\tilde{r}}{kt^{\frac{1}{2}}} \quad , \quad (4.4.8)$$

$$\eta = \frac{\tilde{z}}{kt^{\frac{1}{2}}} \left(\frac{1}{2}R\right)^{\frac{1}{2}} = \frac{\tilde{z}}{(4\nu_{\ell}t)^{\frac{1}{2}}} \quad , \quad (4.4.9)$$

and a new dependent variable $j(\tilde{\alpha}, \eta)$ such that

$$\varphi_b = \frac{k^{\frac{3}{2}}t^{\frac{1}{2}}}{2\tilde{\alpha}} \left(\frac{1}{2}R\right)^{-\frac{1}{2}} j(\tilde{\alpha}, \eta) \quad . \quad (4.4.10)$$

The boundary conditions (4.4.6) and (4.4.7) are satisfied when

$$\left. \begin{array}{l} j = 0 \\ \frac{\partial j}{\partial \eta} = 0 \end{array} \right\} \text{ at } \eta = 0 \quad , \quad (4.4.11)$$

and

$$\frac{\partial j}{\partial \eta} \rightarrow 1 \quad \text{when } \eta \rightarrow \infty \quad . \quad (4.4.12)$$

Equation (4.4.5) becomes

$$\begin{aligned} & \frac{\partial^3 j}{\partial \eta^3} + 2\tilde{\alpha} \frac{\partial^2 j}{\partial \tilde{\alpha} \partial \eta} + 2\eta \frac{\partial^2 j}{\partial \eta^2} - 2 \frac{\partial j}{\partial \eta} + 2 + \frac{1}{\tilde{\alpha}^3} \left[4 \left(\frac{\partial j}{\partial \eta} \right)^2 - 4 - 2\tilde{\alpha} \frac{\partial j}{\partial \eta} \frac{\partial^2 j}{\partial \eta \partial \tilde{\alpha}} + \right. \\ & \left. + 2\tilde{\alpha} \frac{\partial j}{\partial \tilde{\alpha}} \frac{\partial^2 j}{\partial \eta^2} - 2j \frac{\partial^2 j}{\partial \eta^2} \right] = 0 \quad . \quad (4.4.13) \end{aligned}$$

Its form suggests a procedure of successive approximations for large $\tilde{\alpha}^3$.

Putting

$$j = \int_0^{\eta} f_0(\xi) d\xi + \frac{1}{\tilde{\alpha}^3} \int_0^{\eta} f_1(\xi) d\xi + \dots \quad , \quad (4.4.14)$$

the first of the conditions (4.4.11) is satisfied and (4.4.13) becomes

$$\begin{aligned} & \frac{d^2 f_0}{d\eta^2} + 2\eta \frac{df_0}{d\eta} - 2f_0 + 2 + \frac{1}{\tilde{\alpha}^3} \left[\frac{d^2 f_1}{d\eta^2} + 2\eta \frac{df_1}{d\eta} - 8f_1 + 4f_0^2 - 4 \right. \\ & \left. - 2 \frac{df_0}{d\eta} \int_0^{\eta} f_0(\xi) d\xi \right] + \frac{1}{\tilde{\alpha}^6} [\dots] + \dots = 0 \quad , \quad (4.4.15) \end{aligned}$$

with the conditions

$$f_0 = 0, \quad f_1 = 0, \quad \dots \quad \text{at } \eta = 0 \quad , \quad (4.4.16)$$

$$f_0 = 1, \quad f_1 = 0, \quad \dots \quad \text{at } \eta = \infty \quad . \quad (4.4.17)$$

The zero-order solution is

$$f_0 = 1 - \tau^{\frac{1}{2}} \text{ierfc } \eta \quad (4.4.18)$$

where $\text{ierfc } \eta$ denotes the first integral of the complementary error function of η . The homogeneous part of the first-order equation has the solutions $i^4 \text{erfc } \eta$ and $i^4 \text{erfc}(-\eta)$, these being fourth integrals of the complementary error function. The solution of the complete equation can be obtained with the method of variation of the constants. Putting

$$f_1 = A(\eta) i^4 \text{erfc } \eta + B(\eta) i^4 \text{erfc}(-\eta) \quad (4.4.19)$$

we have the conditions

$$\frac{dA}{d\eta} i^4 \text{erfc } \eta + \frac{dB}{d\eta} i^4 \text{erfc}(-\eta) = 0 \quad (4.4.20)$$

$$- \frac{dA}{d\eta} i^3 \text{erfc } \eta + \frac{dB}{d\eta} i^3 \text{erfc}(-\eta) = 4 - 4f_0^2 + 2 \frac{df_0}{d\eta} \int_0^\eta f_0(\xi) d\xi \quad (4.4.21)$$

which determine $dA/d\eta$ and $dB/d\eta$. With two constants, determined by the boundary conditions, $A(\eta)$ and $B(\eta)$ can then be found. To find the thickness of the boundary layer and to determine whether separation will occur in the region $\tilde{\alpha} > 1$, it is not necessary to determine the solution completely.

Separation of the boundary layer is characterized by the reversal of the direction of flow at the solid surface. Thus the point of separation is determined by the condition

$$\left(\frac{\partial v_r}{\partial z} \right)_{z=0} = 0 \quad ,$$

which is equivalent to

$$\frac{df_0}{d\eta} + \frac{1}{\tilde{\alpha}^3} \frac{df_1}{d\eta} = 0 \quad \text{at } \eta = 0 \quad , \quad (4.4.22)$$

when terms containing higher powers of $\tilde{\alpha}^{-3}$ are neglected. Consider the solution (4.4.19) of the first-order equation. As

$$i^4 \operatorname{erfc}(-\eta) \rightarrow \infty \quad \text{for } \eta \rightarrow \infty \quad ,$$

we have

$$B(\infty) = 0$$

in view of (4.4.17). But then

$$B(\eta) = - \int_{\eta}^{\infty} \frac{dB}{d\eta} d\eta \quad , \quad (4.4.23)$$

and as

$$A(0) = -B(0) \quad , \quad (4.4.24)$$

in view of condition (4.4.16) we have

$$A(0) = \int_0^{\infty} \frac{dB}{d\eta} d\eta \quad . \quad (4.4.25)$$

From the conditions (4.4.20) and (4.4.21) we have

$$\frac{dB}{d\eta} = 4 \frac{\{1 - (1 - \pi^{\frac{1}{2}} i \operatorname{erfc} \eta)^2 + \frac{1}{2} \pi^{\frac{1}{2}} \operatorname{erfc} \eta (\eta + \pi^{\frac{1}{2}} i^2 \operatorname{erfc} \eta - \frac{1}{4} \pi^{\frac{1}{2}})\} i^4 \operatorname{erfc} \eta}{i^4 \operatorname{erfc}(-\eta) i^3 \operatorname{erfc} \eta + i^3 \operatorname{erfc}(-\eta) i^4 \operatorname{erfc} \eta} \quad . \quad (4.4.26)$$

Repeated partial integrations, combined with the use of recurrence relations and differentiation formulas for the integrals of the complementary error function, then yield with (4.4.25)

$$A(0) = \frac{248}{15} - \frac{27\pi}{8} \quad . \quad (4.4.27)$$

With (4.4.24) and (4.4.20) we have from (4.4.19)

$$\left(\frac{df_1}{d\eta}\right)_{\eta=0} = -2A(0) i^3 \operatorname{erfc}(0) = -\frac{A(0)}{3\pi^{\frac{1}{2}}} \quad . \quad (4.4.28)$$

The condition for separation (4.4.22) is then

$$\frac{1}{\pi^{\frac{1}{2}}} - \frac{1}{3\pi^{\frac{1}{2}}\tilde{\alpha}^3} \left(\frac{248}{15} - \frac{27\pi}{8} \right) = 0 \quad . \quad (4.4.29)$$

A point of separation is therefore not found in the region $\tilde{\alpha} > 1$ outside the bubble. The result $\tilde{\alpha}^3 \simeq 0.63$ from (4.4.29) is itself meaningless because the analysis is valid outside the bubble only.

The displacement thickness h^* of the boundary layer is defined by the expression

$$h^* = (4\nu_{\ell}t)^{\frac{1}{2}} \int_0^{\infty} \frac{\tilde{v}_{r,m} - \tilde{v}_r}{\tilde{v}_{r,m}} d\eta \quad , \quad (4.4.30)$$

where $\tilde{v}_{r,m}$ is the velocity outside the boundary layer given by (4.4.7), which can be rewritten, if only zero and first-order terms in $\tilde{\alpha}^{-3}$ are retained, as

$$\begin{aligned} h^* &= (4\nu_{\ell}t)^{\frac{1}{2}} \int_0^{\infty} (1 - f_0 - \frac{1}{\tilde{\alpha}^3} f_1) d\eta = \\ &= (4\nu_{\ell}t)^{\frac{1}{2}} \left[\pi^{\frac{1}{2}} \int_0^{\infty} i \operatorname{erfc} \eta \, d\eta - \frac{1}{\tilde{\alpha}^3} \int_0^{\infty} \{A i^4 \operatorname{erfc} \eta + B i^4 \operatorname{erfc}(-\eta)\} d\eta \right] \quad . \quad (4.4.31) \end{aligned}$$

A partial integration of the second integral I_2 yields

$$\begin{aligned} I_2 &= \int_0^{\infty} \{A i^4 \operatorname{erfc} \eta + B i^4 \operatorname{erfc}(-\eta)\} d\eta = \\ &= - \left[A i^5 \operatorname{erfc} \eta - B i^5 \operatorname{erfc}(-\eta) \right]_0^{\infty} + \\ &+ \frac{1}{10} \int_0^{\infty} \left\{ \frac{dA}{d\eta} i^3 \operatorname{erfc} \eta - \frac{dB}{d\eta} i^3 \operatorname{erfc}(-\eta) \right\} d\eta \quad , \quad (4.4.32) \end{aligned}$$

with the use of the recurrence relations and (4.4.20). As $B(\infty) = 0$ and $i^5 \operatorname{erfc}(\infty) = 0$, using also (4.4.24) and (4.4.21), we obtain

$$\begin{aligned} I_2 &= 2A(0) i^5 \operatorname{erfc}(0) - \frac{4}{10} \int_0^{\infty} \left\{ 1 - (1 - \pi^{\frac{1}{2}} i \operatorname{erfc} \eta)^2 + \right. \\ &+ \left. \frac{1}{2} \pi^{\frac{1}{2}} \operatorname{erfc} \eta (\eta + \pi^{\frac{1}{2}} i^2 \operatorname{erfc} \eta - \frac{1}{4} \pi^{\frac{1}{2}}) \right\} d\eta = -\frac{1}{4} \pi^{\frac{1}{2}} \left(\frac{9}{4} - \frac{4\sqrt{2}}{5} - \frac{496}{225\pi} \right) \quad . \quad (4.4.33) \end{aligned}$$

The final result is

$$\frac{h^*}{(4 \nu_l t)^{\frac{1}{2}}} \simeq \frac{1}{4} \pi^{\frac{1}{2}} \left(1 + \frac{0.42}{\tilde{\alpha}^3} \right) \quad (4.4.34)$$

to the first order in $1/\tilde{\alpha}^3$. The zero-order term for the thickness of the boundary layer has been calculated already by Olander and Watts⁴¹, in the way which will be discussed in Section 5.3.

Any residual velocity of the liquid captured under the bubble will be small, as the liquid in the boundary layer is decelerated by the adverse pressure gradient outside the bubble and stopped entirely by the friction forces once under the bubble where no pressure force acts on the liquid. Effects of a residual velocity are taken into account, if the displacement thickness of the boundary layer, by definition the hypothetical thickness of the layer at standstill in a further undisturbed flow field, is used as a measure of the thickness of the liquid layer under the bubble. Doing this we rewrite (4.3.8) with (4.2.44) and (4.3.1) as

$$\frac{h_0(r_b)}{(4 \nu_l t)^{\frac{1}{2}}} = \frac{Z_b}{\sqrt{2}} \quad , \quad (4.4.35)$$

to find, comparing (4.4.35) and (4.4.34) at $\tilde{\alpha} = 1$, that Z_b will be approximately given by

$$Z_b \simeq 0.9 \quad . \quad (4.4.36)$$

Following this approach consistently, we consider in what follows the liquid in the layer under the bubble to be at rest. Changes in the original thickness of the liquid layer given by (4.3.9) will then occur through evaporation only.

This is not exact. Although the total volume of liquid in the microlayer, captured by the moving circumference of the bubble, is given by

$$\int_0^t \frac{dr_b}{dt} h^*(r_b) 2\pi r_b dt = \frac{2}{3} \pi r_b^3 Z_b R^{-\frac{1}{2}} \quad , \quad (4.4.37)$$

evaporation being neglected, the exact distribution $h'(\tilde{r})$ of this amount over the solid surface under the bubble is unknown. Obviously we must have

$$\int_0^{r_b} h'(\tilde{r}) 2\pi\tilde{r}d\tilde{r} = \frac{2}{3}\pi r_b^3 Z_b R^{-\frac{1}{2}} \quad (4.4.38)$$

Note that $h_0(\tilde{r})$, corresponding to zero liquid velocity everywhere in the microlayer, which is given by (4.3.9), satisfies this expression. It is easy to see that a residual velocity of the liquid in the microlayer will result in $h'(\tilde{r})$ being larger than $h_0(\tilde{r})$ in the outer area of the microlayer, and smaller than $h_0(\tilde{r})$ towards the centre. The magnitude of the difference will depend on the rate at which viscous dissipation of the kinetic energy of the residual flow occurs. Considered at a fixed position the microlayer thickness will decrease with time until the flow has stopped. To this decrease we must add the decrease by evaporation which was neglected here. We do not yet know how to handle the problem of residual flow.

4.5. Evaporation of the microlayer and bubble growth rate

The bubble grows under the influence of the superheat by evaporation at both the hemispherical surface and the surface of the thin liquid layer on the solid. In the following we focus our attention on the latter contribution to growth.

Cylindrical polar coordinates \tilde{r} , \tilde{z} , $\tilde{\varphi}$ will again be used, with the positive \tilde{z} -axis coinciding with the axis $\vartheta = 0$ of the spherical polar coordinates used in previous sections. As the liquid layer under the bubble is thin, inside the layer the cylindrical coordinate \tilde{r} can be identified with the spherical coordinate r .

To get an impression of the evaporation process, let us consider what happens locally near the solid-liquid interface at a fixed distance from the centre of the bubble. At the moment when the hemispherical bubble boundary passes this point, a thin layer of liquid is left on the solid surface. The temperature of the liquid is equal to the initial temperature as it has not been in contact with the bubble previously. Once the liquid is under the bubble, evaporation occurs from the top of the layer and the temperature is T_0 there. So, considered locally, the passing of

the bubble boundary starts evaporation for which the necessary heat is supplied by a transient cooling process which after some time penetrates the solid under the layer. Ultimately the liquid layer will be evaporated completely. Obviously convective currents cannot develop in this extremely thin liquid layer, the Rayleigh number being a factor 10^{-5} too small for the onset of free convection to occur.

For rapidly growing bubbles the approach of the hemispherical bubble boundary is felt only slightly ahead of it in the stagnant liquid in contact with the surface of the solid. This implies that the heat conduction process which supplies the heat for the evaporation of the liquid layer takes place almost exclusively under the bubble. But this in turn implies that the rate of supply of heat to the entire vapour-liquid interface of the thin liquid layer is determined by the area of solid surface covered by this layer and the penetration in the negative \tilde{z} -direction towards the solid of the transient heat conduction. As a result the heat conduction can be considered to occur in the z -direction only for a calculation of the total vapour production over the entire surface area of the liquid layer. The temperature gradients in the \tilde{z} -direction can be shown to be a factor $R^{\frac{1}{2}}$ larger than those in the \tilde{r} -direction.

In the following we therefore assume heat diffusion to occur in the \tilde{z} -direction only, both in the solid and in the thin liquid layer. Consider the situation at $\tilde{r} = \tilde{r}_1$. The bubble boundary passes this position at a time $t_1 = \tilde{r}_1^2/k^2$ and at this moment a layer of liquid of thickness

$$h_0 = \tilde{r}_1 Z_b R^{-\frac{1}{2}} \quad , \quad (4.3.9)$$

is left on the solid, after which heat conduction and evaporation start.

The initial conditions are

$$T_\ell = T_s = T_1 \quad \text{at} \quad t = t_1 \quad , \quad (4.5.1)$$

$$h = h_0 \quad \text{at} \quad t = t_1 \quad , \quad (4.5.2)$$

h being the actual thickness of the liquid layer which is a function of both \tilde{r}_1 and t . The boundary conditions are

$$T_{\ell} = T_0 \quad \text{at } \tilde{z} = h \quad , \quad (4.5.3)$$

$$T_{\ell} = T_s \quad \text{at } \tilde{z} = 0 \quad , \quad (4.5.4)$$

$$\lambda_{\ell} \frac{\partial T_{\ell}}{\partial \tilde{z}} = \lambda_s \frac{\partial T_s}{\partial \tilde{z}} \quad \text{at } \tilde{z} = 0 \quad , \quad (4.5.5)$$

$$T_s \rightarrow T_1 \quad \text{when } \tilde{z} \rightarrow -\infty \quad . \quad (4.5.6)$$

The heat diffusion equations are

$$\frac{\partial T_{\ell}}{\partial t} = a_{\ell} \frac{\partial^2 T_{\ell}}{\partial \tilde{z}^2} \quad , \quad (4.5.7)$$

and

$$\frac{\partial T_s}{\partial t} = a_s \frac{\partial^2 T_s}{\partial \tilde{z}^2} \quad . \quad (4.5.8)$$

The rate of change in thickness of the liquid layer is related to the heat flux at the vapour-liquid interface

$$\rho_{\ell} L \frac{dh}{dt} = -\lambda_{\ell} \left(\frac{\partial T_{\ell}}{\partial \tilde{z}} \right)_{\tilde{z}=h} \quad . \quad (4.5.9)$$

The volumetric vapour flux Ω at $\tilde{r} = \tilde{r}_1$ is given by

$$\Omega(r_1) = -\frac{\rho_{\ell}}{\rho_v} \frac{dh}{dt} \quad . \quad (4.5.10)$$

Conditions (4.5.9) and (4.5.10) are equivalent to (4.2.20) when we take into account that the velocity in the liquid layer is zero.

Obviously, the above equations apply only to the time interval when $0 \leq h \leq h_0$, but this is the interval of interest, as the direct conduction of heat from the solid to the vapour which occurs after this interval will be neglected.

All expressions can be brought into a dimensionless form with the help of a reference temperature and a reference length, for which $T_1 - T_0$ and h_0 are chosen, respectively, the latter to obtain the smallest possible number of parameters in the equations. We define the dimensionless thickness of the liquid layer as

$$\beta = \frac{h}{h_0} \quad , \quad (4.5.11)$$

and the dimensionless coordinate in the liquid as

$$\tilde{\eta} = \frac{\tilde{z}}{h_0} \quad , \quad \tilde{z} > 0 \quad , \quad (4.5.12)$$

and in the solid as

$$\tilde{\eta} = \frac{\tilde{z}}{h_0} H^{-\frac{1}{2}} \quad , \quad \tilde{z} < 0 \quad . \quad (4.5.13)$$

The quantity H is defined as

$$H = \frac{a_s}{a_l} \quad . \quad (4.5.14)$$

As dimensionless time we use

$$\tau = \frac{a_l(t - t_1)}{h_0^2} \quad . \quad (4.5.15)$$

The dimensionless temperatures are defined according to (4.2.34) and (4.2.35). Two more dimensionless constants will appear

$$J = \frac{c_l(T_1 - T_0)}{L} \quad , \quad (4.5.16)$$

and

$$M = \frac{\lambda_s}{\lambda_l} \quad . \quad (4.5.17)$$

J is related to the Jakob number $\rho_l c_l (T_1 - T_0) / \rho_v L$; c_l is the specific heat of the liquid.

The expressions defining the problem then become as follows:

$$\theta_l = \theta_s = 1 \quad \text{at } \tau = 0 \quad . \quad (4.5.18)$$

$$\beta = 1 \quad \text{at } \tau = 0 \quad . \quad (4.5.19)$$

$$\theta_l = 0 \quad \text{at } \tilde{\eta} = \beta \quad . \quad (4.5.20)$$

$$\theta_l = \theta_s \quad \text{at } \tilde{\eta} = 0 \quad . \quad (4.5.21)$$

$$\theta_s \rightarrow 1 \quad \text{when } \tilde{\eta} \rightarrow -\infty \quad (4.5.22)$$

$$\frac{\partial \theta_l}{\partial \tilde{\eta}} = MH^{-\frac{1}{2}} \frac{\partial \theta_s}{\partial \tilde{\eta}} \quad \text{at } \tilde{\eta} = 0 \quad (4.5.23)$$

$$\frac{\partial \theta_l}{\partial \tau} = \frac{\partial^2 \theta_l}{\partial \tilde{\eta}^2} \quad (4.5.24)$$

$$\frac{\partial \theta_s}{\partial \tau} = \frac{\partial^2 \theta_s}{\partial \tilde{\eta}^2} \quad (4.5.25)$$

$$\frac{d\beta}{d\tau} = J \left(\frac{\partial \theta_l}{\partial \tilde{\eta}} \right)_{\tilde{\eta}=\beta} \quad (4.5.26)$$

To obtain the last expression the definition of the heat diffusivity

$$a_l = \lambda_l \rho_l^{-1} c_l^{-1} \quad ,$$

was used.

So formulated the problem can in principle be solved for β as a function of τ . The value τ_d of τ for which $\beta = 0$ is then obtained. From the expressions (4.5.18) to (4.5.26) it can be seen that these results depend only on the two constant parameters, J and $MH^{-\frac{1}{2}}$, hence τ_d is a constant. Note that $MH^{-\frac{1}{2}} = \left(\frac{\lambda_s \rho_s c_s}{\lambda_l \rho_l c_l} \right)^{\frac{1}{2}}$ equals the ratio of the contact coefficients for the solid and the liquid.

The vapour flux can be expressed with the help of (4.3.9) as

$$\Omega(r_1) = -K \frac{a_l}{h_0} \frac{d\beta}{d\tau} = - \frac{a_l K R^{\frac{1}{2}}}{Y_1 Z_b} \frac{d\beta}{d\tau} \quad , \quad (4.5.27)$$

where K is defined as

$$K = \frac{\rho_l}{\rho} \quad . \quad (4.5.28)$$

From (4.5.15), (4.3.1) and (4.3.9) we obtain

$$\tau = \frac{a_l R}{k^2 Z_b^2} \frac{r_b^2 - \tilde{r}_1^2}{\tilde{r}_1^2} \quad . \quad (4.5.29)$$

Defining the Prandtl number

$$P = \frac{\nu_{\ell}}{a_{\ell}} \quad , \quad (4.5.30)$$

and using (4.2.44) we can write (4.5.29) as

$$\tau = \frac{1}{2PZ_b^2} \frac{r_b^2 - \tilde{r}_1^2}{\tilde{r}_1} \quad . \quad (4.5.31)$$

To calculate the total rate of vapour production from the liquid layer at a given moment of time the vapour flux $\Omega(\tilde{r}_1)$ must be integrated over the area between the circles of radius r_b and r_d . The latter quantity is the radius of the dry area on the solid surface which is determined by τ_d according to equation (4.5.31).

$$r_d = r_b(1 + 2PZ_b^2\tau_d)^{-\frac{1}{2}} \quad . \quad (4.5.32)$$

As τ_d is a constant, the radius of the dry area is proportional to the radius of the bubble, as has already been found in Section 4.2.

The integral

$$\int_{r_d}^{r_b} \Omega(\tilde{r}_1) 2\pi\tilde{r}_1 d\tilde{r}_1$$

can be converted to the following integral over τ ,

$$- 2 a_{\ell} r_b K P Z_b R^{\frac{1}{2}} \int_0^{\tau_d} (d\beta/d\tau) (1 + 2PZ_b^2\tau)^{-3/2} d\tau \quad ,$$

which is then used to equate the rate of vapour generation to the rate of increase of the bubble volume, to obtain the equivalent of (4.2.29). We find

$$\begin{aligned} 2\pi r_b^2 (dr_b/dt) = & - 2\pi a_{\ell} r_b K P Z_b R^{\frac{1}{2}} \int_0^{\tau_d} (d\beta/d\tau) (1 + 2PZ_b^2\tau)^{-3/2} d\tau + \\ & + 2\pi a_{\ell} r_b (6/\pi)^{\frac{1}{2}} R^{\frac{1}{2}} K J P^{\frac{1}{2}} \quad , \end{aligned} \quad (4.5.33)$$

where the second term on the right-hand side represents the contribution of evaporation at the hemispherical surface. This term has been taken from the corresponding equation for a spherical bubble in an infinite liquid medium, which is

$$4\pi r_b^2 \frac{dr_b}{dt} = 4\pi a_\ell r_b (6/\pi)^{\frac{1}{2}} R^{\frac{1}{2}} KJP^{\frac{1}{2}},$$

as has been derived by Birkhoff et al.²³. On the left-hand side of (4.5.33) the expression $r_b dr_b/dt$ is replaced by Rv_ℓ with the help of (4.2.43) and (4.2.42), and we end up with the result

$$R^{\frac{1}{2}} = -KZ_b \int_0^{\tau_d} (d\beta/d\tau) (1 + 2PZ_b^2\tau)^{-3/2} d\tau + (6/\pi)^{\frac{1}{2}} KJP^{-\frac{1}{2}}. \quad (4.5.34)$$

As the integral is a constant, $R^{\frac{1}{2}}$ is a constant from which the value of the growth constant k can be calculated. To evaluate the integral the solution $\beta = \beta(\tau)$ of the dimensionless heat conduction and evaporation problem must be obtained, which in general can only be done numerically. Some results are discussed in the following section.

4.6. Analytical solution for a special case, a useful approximation

For the special case when

$$MH^{-\frac{1}{2}} = (\lambda_s \rho_s c_s / \lambda_\ell \rho_\ell c_\ell)^{\frac{1}{2}} = 1 \quad (4.6.1)$$

an analytical solution to the dimensionless heat conduction and evaporation problem is known. This problem is a slightly generalized version of the problem of the evaporation of a semi-infinite body of liquid at a plane vapour-liquid interface which has been solved by Knuth⁴². His formulation of the problem is equivalent to equations (4.5.18) to (4.5.26) with the subscripts s and ℓ and the equations (4.5.21) and (4.5.23) missing, as these are trivial when $MH^{-\frac{1}{2}} = 1$. As can be shown most easily by substitution the remaining equations have the self-similar solution

$$\theta = \frac{\operatorname{erfc} C - \operatorname{erfc} \zeta}{\operatorname{erfc} C} , \quad (4.6.2)$$

which depends on only one independent variable ζ ,

$$\zeta = \frac{1 - \tilde{\eta}}{2\tau^{\frac{1}{2}}} , \quad (4.6.3)$$

and one constant parameter C ,

$$C = \frac{1 - \beta}{2\tau^{\frac{1}{2}}} ,$$

which is the solution of the equation

$$J\pi^{-\frac{1}{2}} = Ce^{C^2} \operatorname{erfc} C . \quad (4.6.4)$$

The dimensionless thickness of the liquid layer β is thus given by

$$\beta = 1 - 2C\tau^{\frac{1}{2}} . \quad (4.6.5)$$

This solution applies to the time interval $0 \leq \tau \leq \tau_d$, when $1 \geq \beta \geq 0$. From equation (4.6.5) we see that

$$\tau_d = \frac{1}{4C^2} \quad (4.6.6)$$

and the radius of the dry area on the solid is

$$r_d = \alpha_d r_b \quad (4.6.7)$$

with

$$\alpha_d = (1 + PZ_b^2/2C^2)^{-\frac{1}{2}} . \quad (4.6.8)$$

The integral in equation (4.5.34) can now be evaluated, resulting in

$$R^{\frac{1}{2}} = KZ_b (1 + PZ_b^2/2C^2)^{-\frac{1}{2}} + (6/\pi)^{\frac{1}{2}} KJP^{-\frac{1}{2}} . \quad (4.6.9)$$

For small values of J the value of C is approximately

$$C = J\pi^{-\frac{1}{2}} . \quad (4.6.10)$$

If PZ_b^2 is not too small, we then find

$$R^{\frac{1}{2}} = (2/\pi)^{\frac{1}{2}} KJP^{-\frac{1}{2}} (1 + \sqrt{3}) \quad , \quad (4.6.11)$$

which shows that in this case a fraction $(1 + \sqrt{3})^{-1}$, or approximately 37%, of the total growth rate is caused by the evaporation from the microlayer.

Returning to the general case where $MH^{-\frac{1}{2}}$ differs from 1, we compare the following expressions where the integrals have been split up.

$$1 = - \int_0^1 (d\beta/d\tau) d\tau - \int_1^{\tau_d} (d\beta/d\tau) d\tau \quad (4.6.12)$$

$$R^{\frac{1}{2}} = - KZ_b \int_0^1 (d\beta/d\tau) (1 + 2PZ_b^2\tau)^{-3/2} d\tau - \\ - KZ_b \int_1^{\tau_d} (d\beta/d\tau) (1 + 2PZ_b^2\tau)^{-3/2} d\tau + (6/\pi)^{\frac{1}{2}} KJP^{-\frac{1}{2}}. \quad (4.6.13)$$

The presence of the last term in the second equation which represents the evaporation at the hemispherical surface plays no role in the following discussion.

The evaporating interface can be regarded as a continuous plane heat source at $\tilde{\eta} = 1$ with a negative strength proportional to $\tau^{-\frac{1}{2}}$. For this particular argument we neglect the displacement of the interface by evaporation, this being small compared with the other distances involved. At a distance $\Delta\tilde{\eta}$ from the interface the heat flux increases until it attains a maximum when $\tau = \frac{1}{2}(\Delta\tilde{\eta})^2$ and decreases again thereafter. The position where the local heat flux attains its maximum, sometimes called the top of the primary heat pulse, is thus found at $\Delta\tilde{\eta} = (2\tau)^{\frac{1}{2}}$. When the thermal properties of solid and liquid are different, an image source must be considered to be present at $\tilde{\eta} = -1$ (or alternatively, reflection of the primary heat pulse to occur at the plane $\tilde{\eta} = 0$), with the result that the top of a secondary heat pulse reaches the evaporating interface at $\tau = 2$. At that moment the influence of the thermal properties of the solid on the evaporation will be strong already, but

when $\tau = 1$ it is still negligible, since only about 10% of the energy of the heat source is transported beyond $\Delta\tilde{\eta} = \tau^{\frac{1}{2}}$.

The integrals in the identity (4.6.12) in a sense describe the evaporation of the liquid layer at a fixed position under the bubble in the time interval corresponding to the interval from 0 to τ_d . Those in expression (4.6.13) do so at a fixed moment for all positions under the bubble corresponding to the interval from 0 to τ_d . The value of the first integral in each expression will be independent of the thermal properties of the solid. In (4.6.12) the integral from 0 to 1 will be much smaller than that from 1 to τ_d , since the solid provides the major amount of heat necessary to evaporate the entire liquid layer, the excess enthalpy of the liquid itself only representing a fraction J of the heat necessary for its evaporation. But in (4.6.13) the integral from 0 to 1 may be considerably larger than that from 1 to τ_d when $2PZ_b^2$ is large. The total rate of vapour production at the microlayer which is given by (4.6.13) is not strongly dependent on the thermal properties of the solid therefore, although a large proportion of the heat necessary for complete evaporation of the liquid layer at a fixed point is withdrawn from the solid.

Obviously, the major part of the total rate of vapour production comes from the outer ring of the liquid layer under the bubble, as a consequence of its large area and of the short time elapsed here since the beginning of the transient cooling process. In this region the thermal properties of the solid have not yet influenced the evaporation to any marked extent. The radius of the dry area under the bubble, however, depends strongly on the thermal properties of the solid. Fig. 4.6.1 gives a qualitative sketch of the situation. The contradiction mentioned in Section 3.2 has now been resolved.

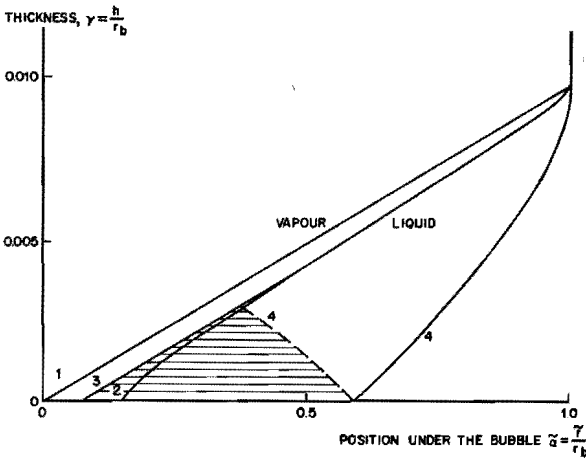


Figure 4.6.1

Qualitative picture of situation under the bubble

- 1 = microlayer surface if no evaporation occurred
- 2 = calculated microlayer surface when $MH^{-\frac{1}{2}} > 1$
- 3 = calculated microlayer surface when $MH^{-\frac{1}{2}} = 1$
- 4 = position where the local heat flux has attained its maximum value ("top of primary or secondary heat pulse")

The influence of the boundary condition at $\tilde{\eta} = 0$ and thus of the thermal properties of the solid is strong in the shaded area.

A direct consequence of this conclusion is the following. In the case when

$$2PZ_d^2 \gg 1 \tag{4.6.14}$$

the best approximation to $d\beta/d\tau$ for calculating the bubble growth rate is one which is accurate for small values of τ . The term $(1 + 2PZ_d^2\tau)^{-3/2}$ in the integrand of the integral in equation (4.5.34) will reduce the error arising from the fact that the approximation is not accurate for larger values of τ .

The approximation

$$(d\beta/d\tau) = -C\tau^{-\frac{1}{2}} \tag{4.6.15}$$

corresponding to the analytical solution (4.6.2) for the case $MH^{-\frac{1}{2}} = 1$ satisfies these requirements. It will be accurate for $0 < \tau < 1$, as discussed in the foregoing. Obviously this approximation cannot be used to calculate τ_d . The expression for the bubble growth resulting from the use of this approximation for $d\beta/d\tau$ is

$$R^{\frac{1}{2}} = C 2^{\frac{1}{2}} KP^{-\frac{1}{2}} (2PZ_b^2 \tau_d)^{\frac{1}{2}} (1 + 2PZ_b^2 \tau_d)^{-\frac{1}{2}} + (6/\pi)^{\frac{1}{2}} KJP^{-\frac{1}{2}} \quad (4.6.16)$$

But as certainly $\tau_d > 1$, and also $2PZ_b^2 \gg 1$, irrespective of the exact value of τ_d we obtain the result

$$R^{\frac{1}{2}} = C 2^{\frac{1}{2}} KP^{-\frac{1}{2}} + (6/\pi)^{\frac{1}{2}} JKP^{-\frac{1}{2}} \quad , \quad (4.6.17)$$

which is also independent of the value of Z_b . This reduces to equation (4.6.11) if C can be approximated by $C = J\pi^{-\frac{1}{2}}$. Numerical solutions for the integral $\int_0^{\tau_d} (d\beta/d\tau)(1 + 2PZ_b^2 \tau)^{-3/2} d\tau$ and τ_d have been determined using an explicit difference scheme and plotted in Figures 4.6.2 and 4.6.3. Figure 4.6.2 indicates the error resulting from the use - as an approximation - of the first term in the right-hand member of (4.6.17). Note that the approximation gives a value which is only 40% smaller than the correct one, even for small Prandtl numbers, when $MH^{-\frac{1}{2}}$ is greatly increased to the value 10. In cases of most practical interest, liquids on metal surfaces, large $MH^{-\frac{1}{2}}$ values often occur. For a Prandtl number $P = 5$ the error is smaller than 25%.

Although the assumption that the heat conduction occurs in the \tilde{z} -direction is entirely justified only if it is used for the calculation of integrals over the whole surface area of the liquid layer, we will use it for a different purpose here. At first sight the approximative treatment in terms of the boundary layer might seem to be unsatisfactory in that it is not clear whether the vapour-liquid interfaces of the thin liquid layer and the hemispherical surface are joined smoothly, especially as the liquid under the bubble is considered to be at rest everywhere, which is not quite realistic here. This point can now be clarified.

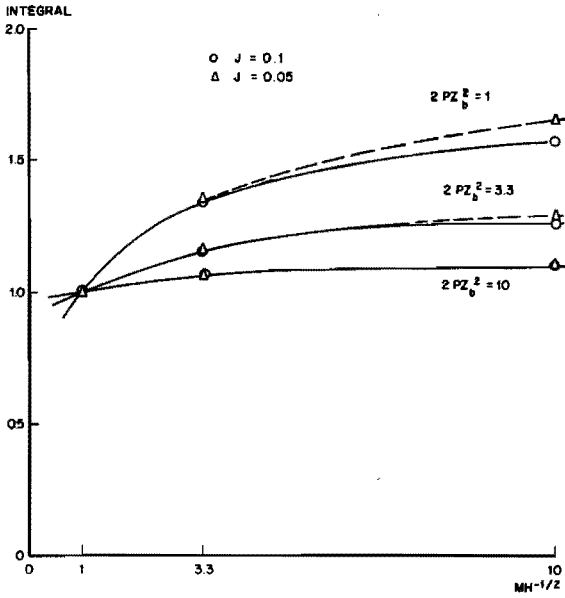


Figure 4.6.2

Value of the integral

$$-(PZ_b^2/2C^2)^{\frac{1}{2}} \int_0^{\tau_d} (d\beta/d\tau)(1 + 2PZ_b^2\tau)^{-\frac{3}{2}} d\tau$$

being the ratio between the results calculated numerically and those obtained with the analytical approximation for the contribution to the bubble growth rate of the evaporation at the microlayer surface

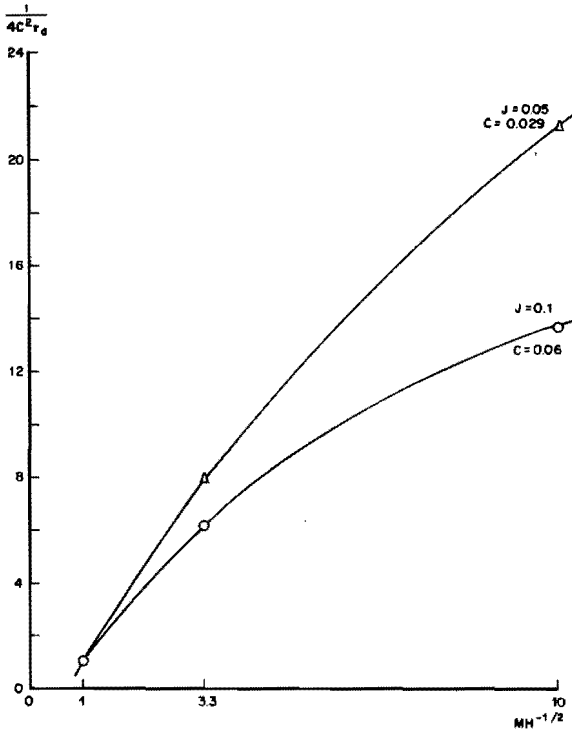


Figure 4.6.3

Numerically calculated values of $(4C^2\tau_d)^{-1}$

τ_d is the dimensionless time for complete evaporation of the microlayer

With the expression (4.6.5) the thickness of the liquid layer under the bubble can be calculated as a function of the distance from the centre of the bubble for $MH^{-\frac{1}{2}} = 1$. Again, for small values of τ , that is near the hemispherical surface, the result will also be valid when $MH^{-\frac{1}{2}}$ is not equal to 1.

From equations (4.6.5), (4.5.11) and (4.5.31) we have

$$\frac{h}{h_0} = 1 - C 2^{\frac{1}{2}} P^{-\frac{1}{2}} Z_b^{-1} \left(\frac{r_b^2}{r_1^2} - 1 \right)^{\frac{1}{2}} \quad (4.6.18)$$

If

$$\gamma = \frac{h}{r_b} = \frac{h}{h_0} \frac{h_0}{r_b} \quad , \quad (4.6.19)$$

is defined as the dimensionless thickness of the layer and

$$\tilde{\alpha} = \frac{\tilde{r}_1}{r_b} \quad , \quad (4.6.20)$$

we have from (4.3.9)

$$\gamma = \tilde{\alpha} Z_b R^{-\frac{1}{2}} - C 2^{\frac{1}{2}} R^{-\frac{1}{2}} P^{-\frac{1}{2}} (1 - \tilde{\alpha}^2)^{\frac{1}{2}} \quad . \quad (4.6.21)$$

If $MH^{-\frac{1}{2}} = 1$ this result is valid for $\alpha_d \leq \tilde{\alpha} \leq 1$, where α_d is the value of $\tilde{\alpha}$ for which $\gamma = 0$, defined in equation (4.6.8). If $MH^{-\frac{1}{2}}$ is not equal to 1, the result is valid only for values of $\tilde{\alpha}$ near 1. We see that $d\gamma/d\tilde{\alpha} \rightarrow \infty$ for $\tilde{\alpha} \rightarrow 1$ from below, so the tangent to the surface of the liquid layer coincides with the tangent to the hemispherical surface where these surfaces meet.

CHAPTER 5

APPLICATION OF THE THEORY TO NUCLEATE POOL BOILING

5.1. Evaporation at the hemispherical surface

In nucleate pool boiling the liquid near a nucleation site is not uniformly superheated. The theory developed in Chapter 4 for the case of initial uniform superheat must be modified therefore to be applicable to boiling. We will discuss the kind of temperature field to be expected and then see how this affects the growth of a bubble. Considered separately, in spherical coordinates, a radial temperature gradient will lead to a deviation of growth from $r_b = kt^{\frac{1}{2}}$ after some time, while a variation of the superheat with ϑ will affect the growth constant k only, already from the beginning of growth however.

In nucleate pool boiling at low pressures with a small constant external heat input there is a large time interval between the nucleation of subsequent bubbles. During this interval the heat removed by the last bubble is replenished from the external source. This heat partly accumulates in the solid, while a relatively small amount is conducted into the liquid, the bulk temperature of the liquid being only slightly above the saturation temperature. When the replacement of the lost heat has been completed, the temperature of the solid will be practically uniform at the value which enables nucleation of the next bubble at the nucleation site on the solid surface. In the liquid we find a temperature gradient, the temperature decreasing from that of the solid to that of the bulk liquid with increasing distance from the solid surface.

Consider the next bubble which emerges from the nucleation cavity. After the initial phase of growth when the dynamical excess pressure inside is at its maximum corresponding to the liquid superheat, it enters the phase of rapid growth. If it is assumed that the bubble grows according to expression (4.3.1), the theory developed in the foregoing can without modification describe the heat conduction and the evaporation at the liquid layer under the bubble. The initial conditions near the

solid-liquid interface are the same as those in Section 4.5, while it can be shown that the influence of the small external heat input is negligible during the phase of rapid growth until the bubble has grown to very large dimensions. But the contribution to growth of the evaporation at the hemispherical surface is different now from the idealized situation considered in Chapter 4, as a result of the temperature gradient in the liquid.

At the hemispherical surface of a bubble growing rapidly at a liquid-solid interface under conditions of uniform initial superheat a radial temperature gradient extends in the liquid approximately to

$$r = r_b + \Delta r_b \quad (5.1.1)$$

where r_b is given by

$$\Delta r_b = (a_l t)^{\frac{1}{2}} = r_b (2RP)^{-\frac{1}{2}} \quad (5.1.2)$$

When there is an initial temperature gradient in the liquid, this will affect the growth relation (4.3.1) when this gradient, which is enhanced in the radial direction by the flow field, becomes comparable in magnitude with the temperature gradient associated with the self-similar solution. The latter decreases with time proportionally to $t^{-\frac{1}{2}}$ in view of (5.1.2), therefore during a short time interval growth will occur according to (4.3.1), after which a deviation from this relation will be observed.

This shows that the liquid layer and the dry area under the bubble can be observed at least in a qualitative way in a suitably designed boiling experiment.

When the deviation from the relation (4.3.1) occurs, the technique reported by Skinner and Bankoff⁴³ could in principle be used to calculate the evaporation at the hemispherical surface. The complicated influence on the microlayer of the changing growth rate is difficult to predict, however, which anyway restricts our attention to the time interval during which $r_b = kt^{\frac{1}{2}}$ holds. But then, as we will see, qualitative arguments suffice.

We now turn our attention to the time interval during which (4.3.1) holds. The value of the constant k in (4.3.1) during this interval will be affected by the presence of an initial temperature gradient at a bubble in nucleate boiling. A bubble emerging from a nucleation cavity has a finite radius before rapid growth starts. At the beginning of growth the liquid at a short distance outside the bubble has a temperature distribution ranging from the temperature of the solid at the base of the bubble to a lower temperature, say \hat{T} , at the top of the bubble. This temperature distribution remains unchanged in the uniformly radial flow field, as the distance between neighbouring liquid volumes at equal distances from the hemispherical bubble boundary increases proportionally to $kt^{\frac{1}{2}}$, while the penetration distance for heat diffusion is proportional to $(a t)^{\frac{1}{2}}$. The ratio of these quantities, which is $(2 PR)^{\frac{1}{2}}$, is large.

This has two consequences. Firstly, if the temperature distribution were known, the rate of vapour generation from the entire hemispherical surface could be calculated when J is replaced by an average dimensionless superheat J' in the last term of equation (4.5.34). A consequence of the geometry of the sphere is that this average can be expressed as

$$J' = \frac{c_\ell}{L} \frac{1}{r_{b,0}} \int_0^{r_{b,0}} (T(z) - T_0) dz \quad (5.1.3)$$

where $r_{b,0}$ is the radius of the bubble at the beginning of rapid growth. Secondly, this temperature distribution can in principle be measured when the bubble has grown to a much larger size than that corresponding to $r_{b,0}$.

5.2. Experimental verification

As we have shown that growth according to (4.3.1) can be observed in nucleate boiling we will discuss here some experimental results as an illustration of the theory developed in the foregoing.

Growth rates of a large number of bubbles growing on the transparent heating surface were determined with the high-speed film camera. The heating surface was of Pyrex glass or Perspex. As liquids we used

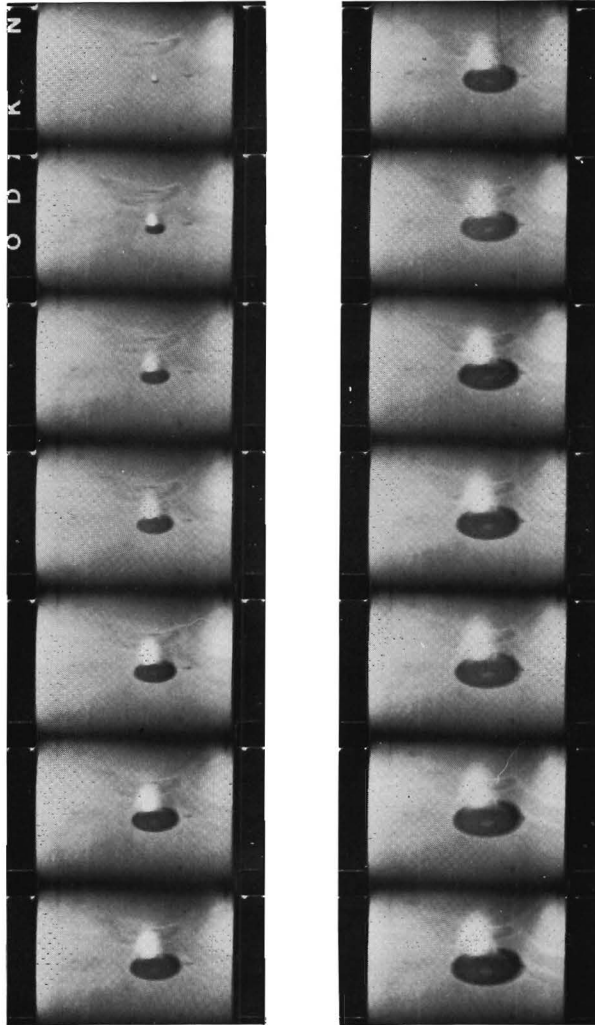


Figure 5.2.1

Growth of a bubble (the first one in Table 5.2.2)
in n-heptane on the pyrex glass plate

Series of frames made with high-speed camera.
The microlayer and dry area under the bubble
are clearly visible. Time between frames 0.288 ms.

n-heptane, benzene and carbon tetrachloride at reduced pressure, when bubbles grow rapidly to a conveniently large size, making observations easier. A number of frames are shown in Fig. 5.2.1.

Plots of the squared bubble radius r_b^2 versus time yielded straight lines over the interval $1 \text{ mm} < r_b < 2 \text{ mm}$ for all bubbles, while for many bubbles the straight lines extended beyond this range (see Fig. 5.2.2). The slope of these lines yields the growth constant. Table 5.2.1 presents the values found and compares them with the results of the approximate analytical calculation, equation (4.6.17), giving also the value of all relevant parameters.

Table 5.2.1

Growth rates of vapour bubbles

Liquid		n-Heptane	n-Heptane	n-Heptane	n-Heptane	Benzene	Carbon tetra- chloride
Heating surface		pyrex	perspex	pyrex	perspex	pyrex	pyrex
Pressure,	kN/m^2	16.6	16.6	24.6	24.6	30	23.3
Boiling point,	K	318	318	329	329	319	308
Superheat,	K	18	19	18	16	26	27
J		0.105	0.11	0.107	0.095	0.108	0.07
$\text{MH}^{-\frac{1}{2}}$		3.3	1.3	3.3	1.3	3.2	4.2
K		1080	1080	755	755	966	1900
P		4.0	4.0	3.8	3.8	4.4	5.5
$R^{\frac{1}{2}}$ anal	$\left\{ \begin{array}{l} J' = 0 \\ J' = \frac{1}{3} J \end{array} \right.$	45	47	33	29	40	45
		71	74	52	46	63	71
$R^{\frac{1}{2}}$ num	$\left\{ \begin{array}{l} J' = 0 \\ J' = \frac{1}{3} J \end{array} \right. Z_b = 0.6$	55	51	41	32	48	52
		81	78	60	49	71	78
$R^{\frac{1}{2}}$ observed	average	82	67	62	52	73	55
Individual values of $R^{\frac{1}{2}}$		78-73-73-75	60-53-72-61	43-94-59	51-53-37		
		115-100-85-92	62-84-75	61-51	46-70-55	70-76	55
		50-70-92-78					

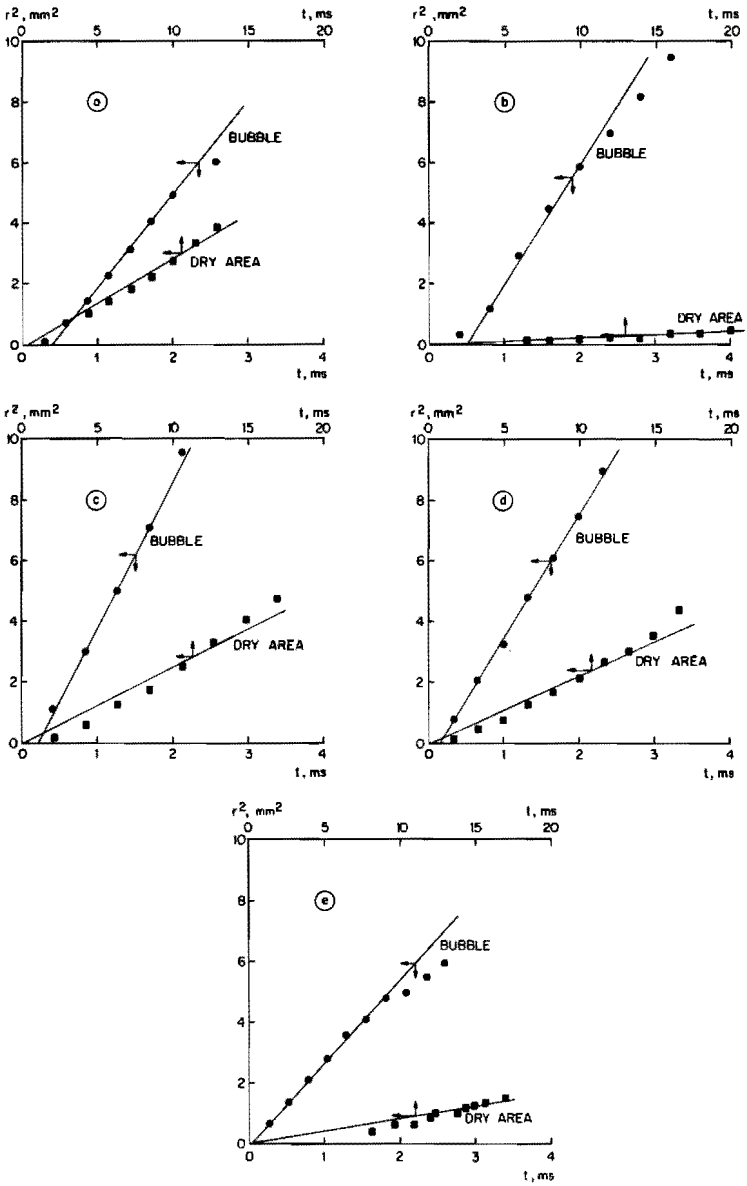


Figure 5.2.2

Squares of bubble and dry area radii as a function of time
for the five bubbles in Table 5.2.2

The results of the numerical solution, obtained from Fig. 4.6.2 with $Z_b = 0.6$, have also been included. The value of J' , defined in (5.1.3), is clearly different for each individual bubble. Temperature measurements in the liquid around the bubbles with the technique described in Section 2.7 confirmed that a higher superheat of the liquid resulted in a higher growth rate. Putting $J' = \frac{1}{3} J$, we obtain reasonable agreement between the calculated growth rate and the average of the values obtained experimentally.

It proved difficult to determine the value of the dimensionless constant Z_b from the ratio of bubble radius and dry area radius with (4.5.32). Measurement from the films of the dry area radius is useful only in the range $1 \text{ mm} < r_d < 2 \text{ mm}$ where the bubble boundary has passed at the velocity corresponding to $r_b = kt^{\frac{1}{2}}$. In this range the original thickness of the microlayer is much larger than the surface roughness, while the transient heat flux required by the rate of evaporation is large compared with the constant electrical heat input of 20 kW/m^2 in our experiments. Many bubbles, especially on perspex, leave the heating surface before the dry area has grown to this size. Straight line plots of r_d^2 versus t could not be obtained, and a straight line had therefore to be drawn from the point corresponding to that where the line for r_b^2 intersects the horizontal axis, matching the plotted data as closely as possible. See the plots of Figure 5.2.2 for the bubbles in Table 5.2.2. Their slope divided by the slope of r_b^2 versus t yields α_d^2 . With the value of τ_d from Figure 4.6.3 Z_b can be calculated from equation (4.5.32). The values obtained for Z_b , between 0.3 and 0.8, are presented in Table 5.2.2. Their order of magnitude agrees with that predicted in Section 4.4. In other cases than those presented in this table no films suitable for measuring the dry area radius were available.

The growth rates, or Reynolds numbers, predicted on the basis of the numerical calculation are not strongly dependent on the value of Z_b because the contribution of the microlayer evaporation to the total growth rate is quite close to the value obtained from the analytical approximation anyway, which is itself independent of Z_b . No conclusions regarding the value of Z_b can be drawn on the basis of observed growth rates therefore, also because of the uncertainty in the value of J' . We have used the value $Z_b = 0.6$, which is in the middle of the range of

observed and calculated values. For a larger value the predicted growth rates $R_{num}^{\frac{1}{2}}$ would be closer to the values $R_{anal}^{\frac{1}{2}}$, predicted by the analytical approximation, which are shown in Table 5.2.1.

Table 5.2.2

		<u>Experimental values of Z_b</u>			
Liquid		n-Heptane	n-Heptane	Benzene	Carbon tetrachloride
Heating surface		pyrex	perspex	pyrex	pyrex
Pressure,	kN/m^2	24.6	16.6	30	23.3
Boiling point,	K	329	318	319	308
Superheat,	K	18	19	26	27
J		0.107	0.11	0.108	0.07
$MH^{-\frac{1}{2}}$		3.3	1.3	3.2	4.2
K		755	1080	966	1900
P		3.8	4.0	4.4	5.5
$R_{num}^{\frac{1}{2}}$	with $J' = \frac{1}{3}J$	60	78	71	78
$R_{observed}^{\frac{1}{2}}$		60	71	76-70	55
α_d^{-2}	$\alpha_{d_{observed}}$	10.5	~160	19-18.2	31
τ_d	from Figure 4.6.3	11	~33	10	17
Z_b	from α_d	0.34	~0.78	0.45-0.44	0.39
Z_b	theor.	~0.9	~0.9	~0.9	~0.9
Plot in Figure 5.2.2		a	b	c-d	e

The discrepancy between the experimental values for Z_b , between 0.3 and 0.8, and the theoretical value of 0.9, might indicate some reduction of the microlayer thickness by residual flow, as discussed in the final paragraphs of Section 4.4. But, owing to the large spread in the experimental values, we cannot regard this discrepancy as substantial evidence that such residual flow in the microlayer is important.

The apparent contradiction that the growth rate is hardly but the dry area radius strongly dependent on the thermal properties of the solid mentioned in Section 3.2 has already been explained in Section 4.6. It is illustrated by the experimental results in Tables 5.2.1 and 5.2.2. Growth rates on pyrex and perspex at the same pressure differ only slightly, not by a factor of 2.5 as would be expected on the basis of equation (3.2.4). Note that the ratio between the values of $(\lambda_s \rho_s c_s)^{\frac{1}{2}}$ of pyrex and perspex is equal to the ratio between the respective values of $MH^{-\frac{1}{2}}$. The very small dry area radius which was observed on perspex is reflected in the large value of α_d^{-2} in Table 5.2.2.

5.3. Comparison of results with literature

In this section some experimental and theoretical results on bubble growth will be critically compared with such results reported in the literature.

As we have seen, the growth relation $r_b = kt^{\frac{1}{2}}$ is accurately confirmed by our experimental results. They are more conclusive in this respect than the experimental results published by Cooper and Lloyd³⁵. The discussion in Section 4.2, which showed that bubble growth at a heating surface occurs according to this relation during the phase of rapid growth, was based on the general equations. No approximations were introduced other than those which explicitly limit the time interval during which rapid growth occurs. The approximations used later in the analysis affect the calculated value of the growth constant k only and not the growth relation. The growth relation has thus been established more generally than in Cooper's³⁶ treatment of the problem, where most approximations are introduced before the growth relation is derived.

An essential difference between Cooper's³⁶ analysis and the present one is that we do not neglect the excess enthalpy of the microlayer liquid. As has been shown in Section 4.6, it is precisely the initial evaporation of the microlayer, in the time interval when the heat for evaporation is still withdrawn from the microlayer liquid only, that is the major factor

which determines the bubble growth rate. This explained the apparent contradiction regarding the influence of the thermal properties of the solid on the growing bubble, and also the fact that the analytical solution for the case $MH^{-\frac{1}{2}} = (\lambda_s \rho_s c_s / \lambda_l \rho_l c_l)^{\frac{1}{2}} = 1$ provides a good approximation of the growth constant, which are both findings confirmed by our experimental results and numerical calculations. The results obtained with both expressions for the growth constant given in Cooper's paper³⁶ can be shown to be incorrect because of the neglected liquid heat content, even when the expressions are applied to the limiting cases for which they are assumed to be exactly valid.

To obtain the zero-order approximation for the thickness of the boundary layer on the solid only a simple calculation is required. A diffusion equation can be found for the difference between main stream and boundary layer velocity by neglecting the convective terms, which are small for small values of time, in the component along the solid surface of the Navier-Stokes equations:

$$\frac{\partial}{\partial t} (\tilde{v}_{r,m} - \tilde{v}_r) = \nu_l \frac{\partial^2}{\partial z^2} (\tilde{v}_{r,m} - \tilde{v}_r)$$

This equation can be solved directly with the boundary conditions (4.4.6) and (4.4.7). With (4.4.30) it then yields the first term of (4.4.34). Note that the continuity equation has not been used, and that the boundary layer thickness found in this way is independent of \tilde{r} . This explains why Cooper and Lloyd³⁵, who carried out this calculation for parallel flow, Mc Sweeney³⁷, who took radial cylindrical flow, and Olander and Watts³⁸, who correctly considered radial spherical flow in the main stream region, all arrived at the same result. But it must be realized that the approximation which was used is valid for small values of time. As this condition is equivalent in the present problem to the condition that $\tilde{\alpha}$ must be large, the result is a zero-order approximation for the microlayer thickness only, which fact is not pointed out in any of the three papers mentioned.

The more elaborate calculations in Section 4.4 give both the zero and first order approximations for the microlayer thickness, but more essential is that they also allow a conclusion to be drawn regarding the possibility of separation of the boundary layer.

For the constant Z_b , which governs microlayer thickness, values between 0.3 and 0.8 were found from our experiments. The values which can be calculated from the experiments of Cooper and Lloyd³⁵ are between 0.4 and 0.7, which compares favourably with our results. As they used an essentially different experimental technique, which is described in Section 3.2, the agreement between their and our results casts some doubt on those obtained by Sharp³⁰ and Jawurek³⁹ who both used optical interference methods to measure microlayer thickness, and deduced values which are an order of magnitude smaller. As mentioned in Section 3.2, it is not certain however whether these values apply to the phase of rapid growth.

5.4. The end of the phase of rapid growth

Various effects suggest themselves as possible causes of the end of the phase of rapid growth. In Section 4.2 we have seen that surface tension and gravity, which should be negligible compared with dynamical effects, become relatively more important with increasing bubble radius. From Figure 4.2.1 it is clear that gravity will be the first to become important for a very rapidly growing bubble, while surface tension will be the first for a bubble growing somewhat more slowly. Both effects will change the shape of the bubble, effectively breaking its contact with the heat supply at the solid surface.

Another possibility is that the slowdown in growth which occurs as a result of the presence of an initial temperature distribution in the liquid leads to a decrease in magnitude of the dynamical effects, which is sufficient to make the influence of either surface tension or gravity felt almost immediately.

But there is still another possibility, which is related to the properties of the flow field in the neighbourhood of the bubble. When growth occurs according to $r_b = kt^{\frac{1}{2}}$, the flow around the bubble is accelerated in the region $r > 2^{1/3} r_b$. As we have seen separation of the boundary layer could not occur, the possible point of separation being found underneath the bubble. When growth slows down, however, the region where the flow is accelerated will be further away from the bubble. The liquid is for example decelerated everywhere when r_b increases less rapidly than proportionally to $t^{1/3}$. As the adverse pressure gradient on the boundary layer will extend over a longer distance separation may now occur. Also when this happens, the bubble boundary will no longer be able to move closely to the solid surface, and the supply of heat will be interrupted.

CHAPTER 6

DRY AREAS AND THE STABILITY OF NUCLEATE AND FILM BOILING

6.1. Experiments on the transition to film boiling

The occurrence of transition to film boiling when the heat flux from the heated surface to a boiling liquid is increased is preceded by the appearance of dry areas on that surface. Their lifetime is much longer than the time interval between nucleation and departure from the heated surface of individual bubbles. In their formation the dry areas in the microlayer of individual bubbles play a role. With our experimental equipment we have determined the nucleate boiling peak heat flux of n-heptane boiling at various pressures. The electrical heat input was increased slowly until a stationary dry area on the heating surface was detected visually, and then switched off again. The maximum heat input was read from a recorder. As such a stationary dry area would grow to cover the entire heating surface if the current is not switched off, the corresponding heat flux is the peak heat flux. At each pressure five values were obtained and averaged. A spread of about 10% between the individual values was normal.

The average values have been plotted against pressure in Figure 6.1.1. A change in the slope of the resulting curve occurs at a pressure of 33.3 kN/m^2 .

High-speed films made through the transparent heating surface at 20.0 kN/m^2 and at atmospheric pressure show a markedly different behaviour of the boiling liquid at the two pressures; see Figure 6.1.2. In both cases dry areas are observed at heat flux values as low as approximately 20% below the peak value.

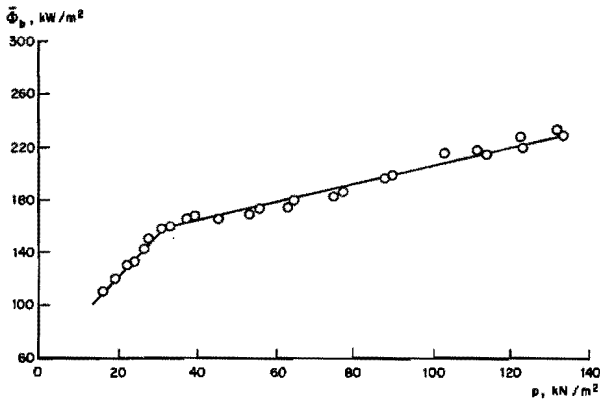


Figure 6.1.1

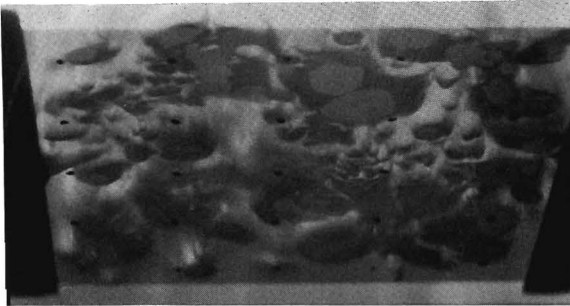
Nucleate boiling peak heat flux as a function of pressure
n-Heptane on pyrex-glass surface, liquid height 50 mm

At atmospheric pressure the dry areas are created by a rather complicated sequence of events. When large numbers of vapour bubbles coalesce near the heating surface at some point they form a large cloud of vapour hovering near the surface. In a thin layer of liquid under the cloud new bubbles nucleate and coalesce with it. The small dry area which occurs under each bubble now remains visible as a tiny dry spot under the cloud of vapour. Evaporation of the liquid in the thin layer causes these dry spots to grow and to merge with neighbouring ones to form much larger dry areas. Normally the solid is wetted again when the increase in buoyancy with size removes the vapour cloud from the vicinity of the heating surface and liquid rushes in. When the heat flux is sufficiently large, suddenly at some point on the heating surface a dry area is not wetted and starts growing, leading to burnout. Even while this occurs the process of formation and disappearance of dry areas continues at other points on the heating surface.

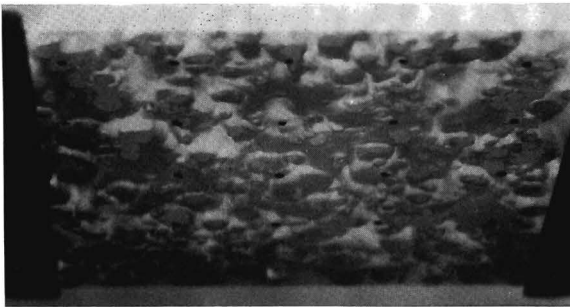
At 20.0 kN/m², the creation of dry areas follows a simpler pattern. Individual bubbles grow to immense size, and so do the dry areas in their microlayer. Sometimes the size of such a dry area is further increased when it merges with that of a second bubble growing from the



Pressure 101.2 kN/m²



Pressure 20.0 kN/m²



Pressure 33.3 kN/m²

Figure 6.1.2

Dry areas and thin films of liquid
on the heating surface at burnout conditions

microlayer within the first. The large dry areas disappear when the bubbles rise from the heated surface. Again, when the heat flux is large enough, suddenly some dry area will not disappear and start growing.

Figure 6.1.2 shows in the first picture the thin layer of liquid under a vapour cloud at atmospheric pressure, with the small dry areas growing and merging. The second photograph shows the large dry areas under individual bubbles, typical of the low-pressure case. Both forms can be observed in the third picture, at a pressure of 33.3 kN/m^2 . This is the pressure at which the slope of the peak heat flux versus pressure curve of Fig. 6.1.1 changes. Unavoidably, still pictures only partly convey the information afforded by the high-speed films.

Surprisingly we found from analysis of the high-speed films that the maximum size and lifetime of dry areas did not change significantly when the heat flux was varied from 80 to 100% of the peak value. The frequency of their occurrence did change, however.

Both the direct observation of the onset of transition and the fact that the change in slope of the curve of Figure 6.1.1 can be closely related to the change in mechanism of dry area formation prove that the dry areas are of vital importance for the occurrence of transition. On the other hand, the occurrence of dry areas of a certain size and lifetime is not sufficient in itself to cause transition, this only being brought about by some dry area satisfying as yet unknown conditions. A further understanding of the transition from nucleate to film boiling clearly requires determination of the nature of these conditions.

6.2. Behaviour of dry areas on a thin wire

A simple model for the study of dry areas is suggested by a boiling experiment, using an electrically heated wire. Such an experiment has been described and analysed by Semeria and Martinet¹⁸. Although our calculations, up to equation (6.2.17), run parallel to one of theirs it should be noted that the underlying interpretation of the boiling curve is entirely different here. Our interpretation leads to different conclusions and only finally returns to the boiling curve to explain its form.

We performed a qualitative experiment only, in which boiling occurred at a long wire submerged in liquid at boiling point. When in this situation the wire is partly removed from the liquid for a few seconds, the non-immersed part will heat up. When the wire is submerged again, two different types of boiling can be observed. In general the point of transition between these regions will move along the wire, but it can be halted by adjustment of the heating current through the wire.

On one part of the wire nucleate boiling occurs, the liquid being in contact with the wire while vapour bubbles are generated in an irregular way. On the other part film boiling occurs, the wire being enveloped by a continuous vapour film from which vapour bubbles are released in the regular pattern characteristic of film boiling. A closer study of the situation at the point between the two regions was made with the high-speed film camera, after the motion of the transition point along the wire had been halted. One frame is shown in Fig. 6.2.1. This study revealed that the point of transition does not move rapidly back and forth but is really stationary, and further that regions of film boiling and nucleate boiling meet directly here. Combining these findings with the fact that the temperature of the wire must be a continuous function of the position along the wire, we can draw the following two conclusions:

- (a) Heat transfer from the wire to the boiling liquid can occur in two different ways corresponding to nucleate and film boiling.
- (b) Above a certain wire temperature, which will be indicated by T_c , film boiling will occur, below T_c nucleate boiling. Contact between liquid and solid will only exist if the temperature of the solid surface is below T_c .

Although T_c will be different for different systems and geometries, it will have a definite value in a given experiment.

Heat transfer and wire temperature will be fluctuating quantities when considered at the level of detail of bubble dimensions and residence times. Here we define the heat flux ϕ and wire temperature T as the average values obtained over an area and time interval which are just so large that the fluctuations are smoothed out. We will further use $\bar{\phi}$ and \bar{T} , the averages over the entire heat transfer surface for the stationary conditions, because the boiling curve is determined in terms of these quantities.

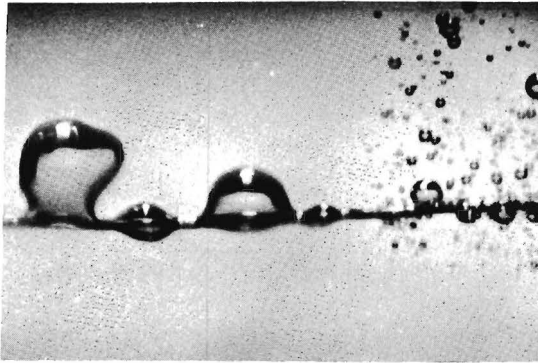


Figure 6.2.1

Film and nucleate boiling on a nichrome wire in n-heptane

With these definitions, for a given set-up, we can assume Φ to be a function of the superheat $T - T_0$ only, which will be discontinuous at $T = T_c$. Where $T > T_c$ film boiling occurs and the heat flux is $\Phi = \Phi_f$; where $T < T_c$ we find nucleate boiling with $\Phi = \Phi_n$. Conceptually this form is attractive as both branches Φ_n and Φ_f can have a positive slope (heat flux increasing with increasing superheat), while the discontinuity at T_c corresponds to a discontinuity clearly observed in experiments.

The two branches Φ_n and Φ_f will obviously to some extent resemble the branches for nucleate and film boiling of the boiling curve. To simplify the mathematical treatment, which is not intended to go beyond a qualitative description here, we will use the simplest form showing this resemblance,

$$\Phi_n = h_n (T - T_0), \quad T < T_c \quad (6.2.1)$$

$$\Phi_f = h_f (T - T_0), \quad T > T_c \quad (6.2.2)$$

with constant h_n and h_f , as depicted in Figure 6.2.2.

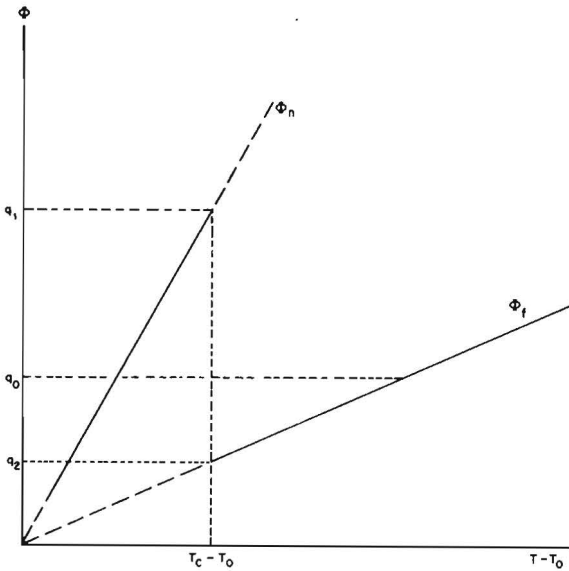


Figure 6.2.2

Local heat flux as a function of local superheat
for locations with nucleate or film boiling

The situation at the long wire of radius r_w is best described in a coordinate system with the origin fixed at the point of transition, which will generally move along the wire at a velocity v in the positive x -direction. Taking the wire to be infinitely long and neglecting temperature differences across its cross-section, we have the following equations and boundary conditions.

$$\pi r_w^2 \rho_s c_s \left(\frac{\partial T}{\partial t} - v \frac{\partial T}{\partial x} \right) = \pi r_w^2 \lambda_s \frac{\partial^2 T}{\partial x^2} + 2\pi r_w (q - \Phi_n), \quad x > 0 \quad (6.2.3)$$

$$\pi r_w^2 \rho_s c_s \left(\frac{\partial T}{\partial t} - v \frac{\partial T}{\partial x} \right) = \pi r_w^2 \lambda_s \frac{\partial^2 T}{\partial x^2} + 2\pi r_w (q - \Phi_f), \quad x < 0 \quad (6.2.4)$$

$$\frac{\partial T}{\partial x} = 0 \quad \text{at } x \rightarrow +\infty \quad (6.2.5)$$

$$\frac{\partial T}{\partial x} = 0 \quad \text{at } x \rightarrow -\infty \quad (6.2.6)$$

$$T = T_c \quad \text{at } x = 0 \quad (6.2.7)$$

$$\frac{\partial T}{\partial x} \text{ continuous at } x = 0 \quad (6.2.8)$$

For convenience the heat generation in the wire is expressed as the amount of heat q generated per unit time and per unit surface area. The boundary condition (6.2.8) excludes the presence of a point source of heat at the origin. Initial conditions have not been stated because we will look for a stationary solution in the moving coordinate system.

With the definitions

$$T_n = \frac{q}{h_n} + T_0 \quad (6.2.9)$$

and

$$T_f = \frac{q}{h_f} + T_0 \quad (6.2.10)$$

the solution which already satisfies all boundary conditions except (6.2.8) is

$$\frac{T - T_n}{T_c - T_n} = \exp \mu_n x, \quad x > 0 \quad (6.2.11)$$

$$\frac{T - T_f}{T_c - T_f} = \exp \mu_f x, \quad x < 0 \quad (6.2.12)$$

where μ_n and μ_f are given by (6.2.13) and (6.2.14).

$$\mu_n = -\frac{v}{2a_s} - \left(\frac{v^2}{4a_s^2} + \frac{2h_n}{r_w \lambda_s} \right)^{\frac{1}{2}} \quad (6.2.13)$$

$$\mu_f = -\frac{v}{2a_s} + \left(\frac{v^2}{4a_s^2} + \frac{2h_f}{r_w \lambda_s} \right)^{\frac{1}{2}} \quad (6.2.14)$$

Here again,

$$a_s = \lambda_s \rho_s^{-1} c_s^{-1} \quad (6.2.15)$$

The boundary condition (6.2.8) leads to the equation

$$\mu_f (T_c - T_f) = \mu_n (T_c - T_n) \quad (6.2.16)$$

which determines v as a function of q .

As a special case, the value of the heat generation corresponding to $v = 0$ is

$$q = q_0 = (h_f h_n)^{\frac{1}{2}} (T_c - T_0) \quad (6.2.17)$$

As mentioned above a similar expression was derived by Semeria and Martinet¹⁸ for one of their approximations to the boiling curve. The situation at the wire is shown qualitatively in Figure 6.2.3. Of the heat generated in the region $x < 0$ only a small amount can be given off directly to the vapour near $x = 0$ at the existing wire temperature, the excess is conducted to the region $x > 0$ to be given off to the liquid there. When insufficient heat can be transferred the remainder, which corresponds to the difference between the areas I and II, will heat the wire near the point of transition, thus extending the region of film boiling.

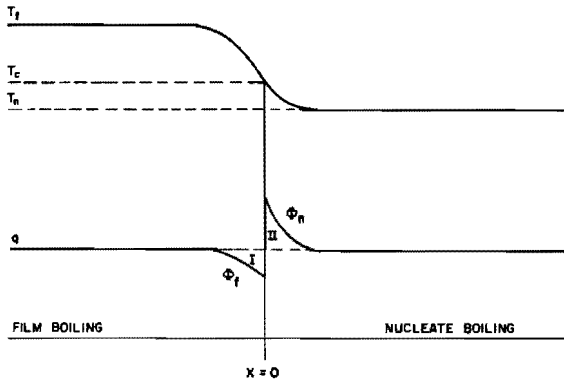


Figure 6.2.3

Temperature profile and heat flux on a wire
with simultaneous film boiling and nucleate boiling

When film boiling occurs over a short length of wire only, a second transition point is present near the first. The excess heat produced in the region of film boiling can now be compensated by conduction to the regions of nucleate boiling at both ends.

It will be shown that a stationary situation with two points of transition requires their distance to be smaller according as the heat generation q is larger. This dependence, a consequence of the interaction between the two points of transition, went unnoticed in the paper by Semeria and Martinet¹⁸. Although this situation is one of unstable equilibrium, as will be discussed in the following, it can be analysed as a stationary condition, as any equilibrium, to determine the critical length of a dry region as a function of q .

For a stationary situation, film boiling occurring over a length of wire $2s_f$ symmetric with respect to the origin, we have the following equations and boundary conditions.

$$0 = \pi r_w^2 \lambda_s \frac{\partial^2 T}{\partial x^2} + 2\pi r_w \left\{ q - h_n (T - T_0) \right\}, \quad x \geq s_f \quad (6.2.18)$$

$$0 = \pi r_w^2 \lambda_s \frac{\partial^2 T}{\partial x^2} + 2\pi r_w \left\{ q - h_f(T - T_0) \right\}, \quad 0 \leq x \leq s_f \quad (6.2.19)$$

$$\frac{\partial T}{\partial x} = 0 \text{ at } x = 0 \quad (6.2.20)$$

$$\frac{\partial T}{\partial x} = 0 \text{ at } x = \infty \quad (6.2.21)$$

$$T = T_c \text{ at } x = s_f \quad (6.2.22)$$

$$\frac{\partial T}{\partial x} \text{ continuous at } x = s_f \quad (6.2.23)$$

All equations and conditions except (6.2.23) are satisfied by

$$\frac{T - T_f}{T_c - T_f} = \frac{\cosh \left(\frac{2h_f}{\lambda_s r_w} \right)^{\frac{1}{2}} x}{\cosh \left(\frac{2h_f}{\lambda_s r_w} \right)^{\frac{1}{2}} s_f}, \quad 0 \leq x \leq s_f \quad (6.2.24)$$

and

$$\frac{T - T_n}{T_c - T_n} = \frac{\exp - \left(\frac{2h_n}{\lambda_s r_w} \right)^{\frac{1}{2}} x}{\exp - \left(\frac{2h_n}{\lambda_s r_w} \right)^{\frac{1}{2}} s_f}, \quad x \geq s_f \quad (6.2.25)$$

Application of the condition (6.2.23) then yields

$$(T_c - T_f) \left(\frac{2h_f}{\lambda_s r_w} \right)^{\frac{1}{2}} \tanh \left(\frac{2h_f}{\lambda_s r_w} \right)^{\frac{1}{2}} s_f = - (T_c - T_n) \left(\frac{2h_n}{\lambda_s r_w} \right)^{\frac{1}{2}}, \quad (6.2.26)$$

or

$$\frac{h_f^{\frac{1}{2}}(T_c - T_0 - q/h_f)}{h_n^{\frac{1}{2}}(T_c - T_0 - q/h_n)} = -\tanh^{-1} \left(\frac{2h_f}{\lambda_s r_w} \right)^{\frac{1}{2}} s_f, \quad (6.2.27)$$

which determines the length of an isolated region of film boiling which is in (unstable) equilibrium, as a function of q .

As limiting cases we have

$$s_f = 0 \quad \text{when} \quad q = q_1 = h_n(T_c - T_0), \quad (6.2.28)$$

$$s_f = \infty \quad \text{when} \quad q = q_0 = (h_f h_n)^{\frac{1}{2}} (T_c - T_0) \quad . \quad (6.2.29)$$

Note that equation (6.2.27) is valid only when $q_0 \leq q \leq q_1$, which implies that situations as considered can have a stationary solution under this condition only. s_f decreases with increasing q . Figure 6.2.4 shows the dependence of s_f on q for a specific case. See Section 6.5.

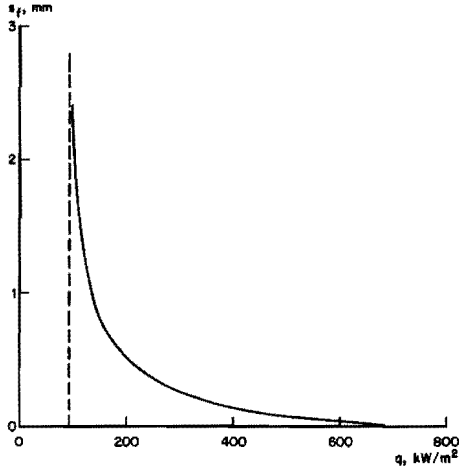


Figure 6.2.4

Critical size of a dry area on a wire as a function of heat generation for a specific case

To establish that the stationary situation is an unstable equilibrium we consider the case of a fixed heat generation q between q_0 and q_1 , and write temporarily s_f^* for the corresponding value s_f given by (6.2.27).

We introduce hypothetical continuous heat sources inside the wire of strength N per unit time at the transition points, replacing (6.2.23) by

$$\lambda_s \left(\frac{\partial T}{\partial x} \right)_f - \lambda_s \left(\frac{\partial T}{\partial x} \right)_n = \frac{N}{\pi r_w^2} \quad \text{at} \quad x = s_f \quad . \quad (6.2.30)$$

Owing to their presence stationary situations can now exist for values s_f differing from s_f^* , which corresponds to $N = 0$. For these stationary situations the temperature profiles are given by (6.2.24) and (6.2.25), which satisfy all boundary conditions except (6.2.23). In its place condition (6.2.30) now requires

$$(T_c - T_f) \left(\frac{2h_f}{\lambda_s r_w} \right)^{\frac{1}{2}} \tanh \left(\frac{2h_f}{\lambda_s r_w} \right)^{\frac{1}{2}} s_f + (T_c - T_n) \left(\frac{2h_n}{\lambda_s r_w} \right)^{\frac{1}{2}} = \frac{N}{\pi r_w^2} \quad (6.2.31)$$

and determines N for a given s_f .

It is easily verified that N is a monotonously decreasing function of $s_f - s_f^*$ which is zero when $s_f = s_f^*$. When $s_f > s_f^*$, heat which should be taken up by the hypothetical sources of negative strength to make the situation a stationary one, is actually available to increase the temperature of the wire, thereby increasing s_f . Then still larger sources of negative strength would be required to render the new situation a stationary one. Thus a dry area larger than s_f^* will continue to grow, and similarly one smaller than s_f^* will disappear. The value s_f^* , which corresponds to the value s_f given by (6.2.27), is therefore the length of a dry region in unstable equilibrium.

A different argument which shows that the equilibrium is unstable, with respect to small changes in q instead of small changes in length, was given by Semeria and Martinet¹⁸. They did not point out the dependence of the equilibrium size on heat generation, however, as does our equation (6.2.27).

The expression corresponding to (6.2.27) for the case of a circular area with radius s_f of film boiling surrounded by nucleate boiling on one side of a thin plate of thickness d insulated on the other side is

$$\frac{h_f^{\frac{1}{2}} (T_c - T_0 - \frac{q}{h_f})}{h_n^{\frac{1}{2}} (T_c - T_0 - \frac{q}{h_n})} = - \frac{I_0 \left\{ \left(\frac{h_f}{\lambda_s d} \right)^{\frac{1}{2}} s_f \right\} K_1 \left\{ \left(\frac{h_n}{\lambda_s d} \right)^{\frac{1}{2}} s_f \right\}}{I_1 \left\{ \left(\frac{h_f}{\lambda_s d} \right)^{\frac{1}{2}} s_f \right\} K_0 \left\{ \left(\frac{h_n}{\lambda_s d} \right)^{\frac{1}{2}} s_f \right\}} \quad (6.2.32)$$

I_n and K_n denote modified Bessel functions of the first and second kind of order n . The arguments for the case of a wire hold equally well for a plate. This parallel also applies to the following sections.

6.3. Thermal stability of the two boiling mechanisms

An interesting aspect of the treatment given above is that the arguments are also valid for an isolated region of nucleate boiling on a wire or plate with film boiling occurring on the remaining part of the surface. For such a region of length $2s_n$ on a wire the condition corresponding to (6.2.27) is

$$\frac{h_n^{\frac{1}{2}}(T_c - T_0 - q/h_n)}{h_f^{\frac{1}{2}}(T_c - T_0 - q/h_f)} = -\tanh^{-1} \left(\frac{2h_n}{\lambda_s r_w} \right)^{\frac{1}{2}} s_n \quad (6.3.1)$$

As limiting cases we have here

$$s_n = 0 \quad \text{when} \quad q = q_2 = h_f(T_c - T_0) \quad (6.3.2)$$

$$s_n = \infty \quad \text{when} \quad q = q_0 = (h_f h_n)^{\frac{1}{2}}(T_c - T_0) \quad (6.3.3)$$

(6.3.1) is thus valid when $q_2 \leq q \leq q_0$.

The region of nucleate boiling in unstable equilibrium is clearly larger for larger values of q .

These findings can be used to determine under what conditions nucleate and film boiling are stable. When $q < q_0$ nucleate boiling is stable, any dry area which is created, no matter how large, will disappear and nucleate boiling is restored. When $q_0 < q < q_1$, small dry areas will disappear, but one which is larger than the critical size will grow, spreading film boiling over the entire wire area. Nucleate boiling is metastable under these conditions, stable with respect to small perturbations but unstable to large ones. When $q > q_1$ nucleate boiling is unstable and will not occur. At $q = q_1$ already the critical size for dry areas is zero. In the same way it is found that film boiling is stable when $q > q_0$, metastable when $q_2 < q < q_0$ and unstable when $q < q_2$. This behaviour has been indicated in Figure 6.3.1.

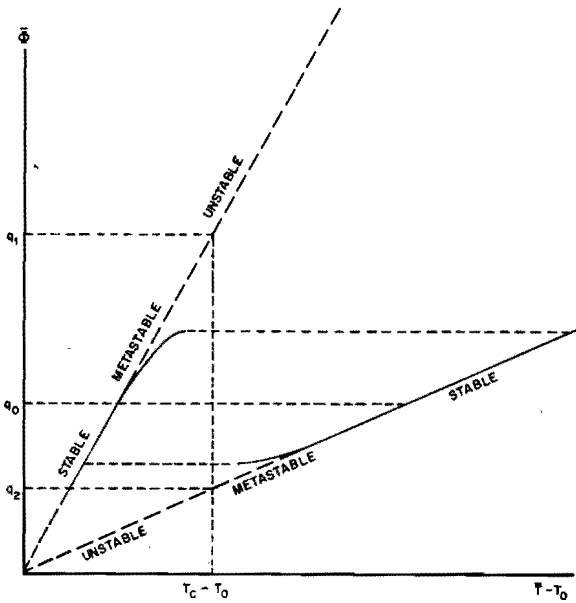


Figure 6.3.1

Construction of boiling curve
Stability of boiling mechanisms

6.4. Construction of the boiling curve

When nucleate boiling occurs over the entire area of a heating surface, this will persist into the metastable region when the heat generation is increased above q_0 . When the heat flux is further increased the formation of dry areas on the heated surface, according to one of the mechanisms described in Section 6.1, will begin and become more and more prominent. At the same time the critical size s_f for a dry area decreases. Before q reaches the value q_1 some dry area will exceed the critical size and cause transition to film boiling. From the curve $\Phi_n = h_n (T - T_0)$ one branch of the boiling curve can now be constructed. The average heating surface temperature will rise slightly above the value $T = q/h_n + T_0$ owing to the intermittent presence of dry areas,

before transition occurs. The branch of the boiling curve representing nucleate boiling will therefore have the form shown in Figure 6.3.1.

When film boiling has been fully established, decreasing the heat generation q will ultimately bring about transition from film boiling to nucleate boiling, at the latest when the value q_2 is reached below which film boiling is unstable (thermally, in the sense used above). Clearly we have hysteresis between the transitions, which agrees with experience.

Although experimental evidence is lacking, one can assume that the hydrodynamical instabilities which, as shown by Chang⁵, determine the release of bubbles from the vapour film in the familiar regular pattern, will also lead to intermittent motion of liquid towards the heating surface. The conditions deciding whether a slug of liquid will establish contact with the hot solid are unknown at present, but simple experiments show that this contact is established intermittently at an initial solid temperature above T_c , before a growing wetted area is observed. Assume for the moment that a temperature T_c^* of the solid exists, only below which contact can be established. With this definition T_c^* can be called the Leidenfrost temperature. Once contact has been established further developments will be determined by the heat generation at the surface and the size of the wetted area. Wetted areas smaller than the critical size will disappear again. The critical size s_n decreases with decreasing q , so before the value q_2 has been reached some wetted area of local nucleate boiling will exceed the critical size and grow, causing transition from film boiling to nucleate boiling.

Before transition occurs, the intermittent presence of wetted areas will decrease the average temperature of the heating surface. The second branch of the boiling curve can now also be indicated qualitatively in Figure 6.3.1. For clarity the two branches have been drawn with slopes less extreme than would be realistic. A curve having the familiar form of the boiling curve results from these arguments; compare Figures 1.3.1 and 6.3.1.

Using special arrangements whereby the heat flux which is transferred to the boiling liquid can sharply decrease locally when superheat increases and vice versa, the transition cannot develop completely. A mixed form of nucleate and film boiling will occur and a curve connecting the two branches of Figure 6.3.1 will be found. That such a curve is found is the result of the definition of the boiling curve as the relationship between the averages $\bar{\Phi}$ and \bar{T} . Stephan⁴⁴ has succeeded in determining such heat flux versus temperature curves for this so-called transition boiling, but a visual description of the boiling behaviour under these conditions is not given in his paper.

The heating surface temperature T_c^* , below which liquid can establish contact with this surface, can be connected in a tentative way with the temperature T_c , the maximum temperature at which nucleate boiling can occur locally. On contact of a slug of liquid, at the saturation temperature T_0 , with a solid at temperature T^* a contact temperature T_i will be established momentarily at the interface, given by

$$\frac{T_i - T_0}{T^* - T_i} = \left(\frac{\lambda_s \rho_s c_s}{\lambda_l \rho_l c_l} \right)^{\frac{1}{2}}, \quad (6.4.1)$$

independent of the heat generation as this is negligible in the short time interval concerned. Putting T_c for the maximum value of T_i , we find a maximum value of T^* which would be T_c^*

$$T_c^* - T_0 = (T_c - T_0) \left\{ 1 + \left(\frac{\lambda_l \rho_l c_l}{\lambda_s \rho_s c_s} \right)^{\frac{1}{2}} \right\}. \quad (6.4.2)$$

It cannot be said whether one of these values T_c and T_c^* is more fundamental than the other from a physical point of view. As this calculation of T_c^* is based on non-stationary considerations and the calculation of the critical size of a wetted area, which governs the development of the situation after such contact, on stationary considerations, at present only a qualitative connection can be established between these two stages.

Another difficulty associated with the present view on T_c^* concerns that part of a surface where film boiling occurs, near for instance a stationary point of transition, where the solid temperature is between T_c and T_c^* . At first sight liquid contact might also occur there, but this is not in accordance with our observations. A comparison between the situation in this narrow region and the situation at a point where liquid establishes a first contact in a region of film boiling does not seem to be justified as hydrodynamical conditions will be markedly different.

The summing up of events leading to the transition from nucleate to film boiling, begun in Section 6.1, can now be completed: When the coalesced vapour leaves the heating surface liquid will wet the solid where its temperature is below T_c^* , whereas hotter areas, those which were dry earlier, are left dry. These will disappear when they are smaller than the critical size, but grow and cause transition when they exceed it.

6.5. Numerical example

In the experiments with n-heptane on our pyrex glass heating surface of 20 mm thickness, the dry areas leading to transition started their growth with a radius of approximately 2.5 mm. From the observed lifetimes of approximately 50 ms of dry areas which disappeared again we can estimate the temperature T_c^* above which the liquid can no longer directly come into contact with the dry solid. When a dry area is formed on the heating surface, the heat generated at the surface cannot be transferred to the liquid and accumulates in the solid. The rise in temperature is approximately given by

$$T(t) - T(0) = 2qt \frac{1}{2} (\pi \lambda_s \rho_s c_s)^{-\frac{1}{2}} \quad (6.5.1)$$

With $q = 200 \text{ kW/m}^2$ we find a rise of 34 K. Combined with the average superheat of 10 K measured at that heat flux we then have $T_c^* - T_0 = 44 \text{ K}$. As $(\lambda_s \rho_s c_s / \lambda_l \rho_l c_l)^{\frac{1}{2}} = 3.4$ equation (6.4.2) yields $T_c - T_0 = 34 \text{ K}$.

From the values of superheat and heat generation we estimate $h_n = 20 \text{ kW/(m}^2 \text{ K)}$. It is known that after burnout in organic liquids the final temperatures are not excessive, say 500 K above the boiling point. This corresponds to $h_f = 0.4 \text{ kW/(m}^2 \text{ K)}$.

Calculating the critical size from (6.2.31), with $\lambda_s = 1.34$ W/m K and $d = 20$ mm we find $s_f \approx 6.8$ mm for the radius of the dry area of critical size. This is of the right order. As the assumption of uniform temperature across the thickness of the heating surface is not valid for this particular heating surface, the calculated value is a rough estimate only. The result for s_f is only weakly affected by the value of h_f which is used. A h_f value of 0.1 kW/m² K corresponding to a post-burnout temperature of 2000 K above boiling point, would lead to $s_f \approx 6.3$ mm.

With the values used above we can calculate the critical size of the dry area on a wire with a diameter of 0.2 mm and a heat conductivity of 15 W/m K, which is shown as a function of heat generation in Figure 6.2.4. If the size of dry areas created were not dependent on q , a higher burnout heat flux would be found on a thicker wire, the critical size being larger for equal q . This tendency has been observed for all but the smallest wire diameters by Van Stralen and Sluyter⁴⁵.

The peak heat flux will be affected by changed conditions in two ways. When the size of dry areas, which are created as described in Section 6.1 would increase, the critical size for transition will be reached at a lower value of q . Changes in the thermal properties of the solid will affect the relationship between critical size and q . The peak heat flux will increase with conductivity for those solid-liquid combinations for which $(\lambda_s \rho_s c_s / \lambda_l \rho_l c_l)^{\frac{1}{2}} \gg 1$, as the critical size s_f is proportional to $\lambda_s^{\frac{1}{2}}$ for a given q . For other combinations the larger value of $(\lambda_s \rho_s c_s / \lambda_l \rho_l c_l)^{\frac{1}{2}}$ for larger λ_s will counteract this tendency, as larger parts of the original dry areas cannot be contacted by the liquid over-running them just after their creation, T_c^* being closer to T_c .

Similarly, the minimum heat flux will be smallest for solids of high conductivity. When $(\lambda_s \rho_s c_s / \lambda_l \rho_l c_l)^{\frac{1}{2}}$ is also large this effect will be enhanced. A comparison with results in the literature is virtually impossible because experiments under similar hydrodynamic conditions offer the only basis for comparison, in view of the important influence of such effects. No contradictory results are known to us.

6.6. Limitations of the analysis

Although the description of the transition from nucleate to film boiling presented here cannot pretend to yield reliable quantitative results, because many simplifications were necessary, it does show that thermal stability is a factor determining the nucleate boiling peak heat flux and causes the hysteresis between nucleate and film boiling. The existence of not more than two different boiling mechanisms is needed to explain the observed behaviour of a boiling liquid.

The discussion has been based somewhat arbitrarily on the existence of a maximum local liquid temperature T_c , the maximum temperature of a solid at which liquid can be in contact with it. This is a quantity which is itself not understood, an objection which can also be raised against the central position given to the peak heat flux in more conventional discussions of the boiling process, to which our treatment offers an alternative.

Clearly we cannot consider the treatment to be more than a first step towards a full understanding of the transition to film boiling. Nevertheless the argument presented here, which connects a number of different aspects of the boiling process, might provide a framework on which further work can be based.

CHAPTER 7

CONCLUDING REMARKS AND SUGGESTIONS FOR FUTURE WORK

It is clear that both problems discussed in this thesis, i.e. bubble growth and dry area behaviour, offer scope for further work. Determination of the residual velocity in and the exact shape of the microlayer would be interesting.

Bubble growth at a liquid-solid interface in a dilute binary mixture is a problem which is in principle equivalent to the present one. Diffusion of the volatile component introduces another differential equation to the problem with a number of homogeneous boundary conditions. If all physical constants are functions of temperature and concentration only, the general structure of the problem would still allow a self-similar solution with growth according to $r_p = kt^{\frac{1}{2}}$, when surface tension effects can be neglected. For the appropriate boundary conditions and the relationship between interface concentration, pressure and temperature we refer the reader to Scriven's¹⁴ paper on the growth of a spherical bubble in the bulk of a binary liquid mixture. The average vapour composition in the bubble will not change, but the concentration and temperature in the liquid at the inner part of the microlayer surface will vary with the position relative to the bubble hemispherical boundary. The resulting surface tension gradient might cause flow in the microlayer to which only viscous forces can offer resistance. Note that the dry area at the bubble centre need not be present in a binary mixture.

Although a fairly complete verbal description of the onset of transition to film boiling is available, major obstacles prevent a better understanding. The coalescence of vapour bubbles, which has hardly received attention in the literature, is a more complicated problem than that of the coalescence of soap bubbles, which has been investigated in more detail. Intermediate equilibrium situations involving Plateau's border cannot exist for coalescing vapour bubbles.

If a conclusion were available regarding the mechanism that brings about the end of the period of rapid growth, the amount of heat carried

away by a bubble could be calculated as a function of its growth constant. As we have seen, this in turn depends on the initial superheat, which is determined by the radius of the nucleation cavity. In combination with knowledge of the waiting time and the size distribution of nucleation cavities the first steps towards a calculation of the rate of heat transfer to a boiling liquid as a function of superheat could then be made.

In an entirely different way there is a possible connection between the mechanism controlling the end of growth of a bubble and the two mechanisms of transition to film boiling at low and normal pressures. Both the single bubble underneath which transition sets in at low pressures and the cloud of coalesced vapour under which it occurs at higher ones, will leave the heating surface under the influence of gravity. As the growth rate of individual vapour bubbles becomes larger when going towards lower pressures, below a certain pressure the end of their period of growth will probably be governed by effects of gravity instead of surface tension, see Figure 4.2.1. The pressure at which this occurs could also be the pressure at which the single bubble mechanism for transition to film boiling becomes predominant.

That the growth rate of individual bubbles becomes larger at lower pressures has two causes. The vapour density decreases with decreasing pressure and the initial superheat, which is the superheat necessary for nucleation, increases with decreasing pressure. This can be seen from equation (1.4.3), when it is combined with the equation of state for an ideal gas.

A further study of the present ideas on the transition to film boiling is necessary. Experiments on dry areas stabilized on a wire with a locally smaller diameter might be useful in this respect.

Further work in these directions may deepen the understanding of the complex phenomena observed in a boiling liquid.

SUMMARY

In this thesis the results are presented of a study of some important phenomena which can occur in pool boiling. In more complicated forms of boiling, such as convective and subcooled boiling, these phenomena are also of great interest. The nucleation of vapour bubbles takes place in cavities at the heating surface and the bubbles therefore grow near a solid surface. Among the consecutive growth phases that of rapid growth is considered in detail. During this phase the growth rate is governed by the transport of heat to the bubble, while the bubble volume increases by several orders of magnitude. The other aspect considered is the transition from nucleate to film boiling which occurs when the heat flux is increased to a high value. An insulating film of vapour is then formed between the liquid and the heating surface.

To study these phenomena experimentally we developed a transparent heating surface consisting of a ground glass or perspex plate with a thin electroconductive film deposited on it. This film served as a heating element. Observations were made through a glass prism with a high-speed camera. In this way the presence of thin liquid layers and dry areas on the heating surface could be detected.

It is known that at low pressures bubbles grow as hemispheres on the heating surface, vapour being generated by evaporation of a thin liquid film, the microlayer, which is present underneath each bubble. A dry area occurs near the centre of the bubble where the microlayer has evaporated entirely. In our experiments these aspects of the growth process could be observed directly. A series of experiments with heating surfaces of the two materials used led us to two conclusions, which at first sight appeared to be contradictory. The bubble growth rate depended hardly on the thermal constants of the solid, but the size of the area where the microlayer had evaporated entirely increased markedly with the value of the contact coefficient of the solid.

From a theoretical analysis we concluded that growth in this form is described by a self-similar solution. In a general way, without it being necessary to obtain the solution, this analysis shows that the shape of

a bubble does not change during growth and that the square of its radius increases proportionally with time. The formation of the microlayer is due to the capture underneath the bubble of liquid from the boundary layer on the solid surface. We studied the flow field around the bubble to show that separation of the boundary layer does not occur, which demonstrates that microlayer formation is possible. Expressions were derived for the zero and first-order terms of the thickness of the boundary layer, which determines the thickness of the microlayer.

In the description of microlayer evaporation for the calculation of the bubble growth rate we explicitly took into account the excess enthalpy of the superheated liquid. For the case in which the contact coefficients of solid and liquid are different we determined the growth rate and dry area radius by numerical calculation. An analytical solution is presented for the case of equal contact coefficients.

Complete evaporation of the microlayer requires a large amount of heat to be withdrawn from the solid, but the expression for the bubble growth rate shows that the initial evaporation practically determines this rate. This initial evaporation is governed by heat withdrawn from the microlayer liquid only. These findings explain why the growth rate of a bubble is hardly affected by the thermal constants of the solid, although the radius of the dry area under the bubble strongly depends on them. The analytical solution therefore provides an approximation for the growth rate, but not for the dry area radius. The constant ratio of dry area to bubble radius, predicted as a consequence of the unchanging shape of a bubble, and the theoretical values of growth rate and microlayer thickness were confirmed by the experiments.

When the nucleate boiling peak heat flux and the transition to film boiling are approached a large number of areas are observed where the heating surface is dry for short intervals. Most dry areas disappear until the odd one suddenly grows to cause transition to film boiling. A simplified analysis was developed of the thermally unstable behaviour of such dry areas, based on an interpretation of the connection between heat transfer and the boiling curve which differs from that encountered usually. We found that the dry areas will grow when they are larger

than a critical size, and disappear when they are smaller. The dependence of this critical size on heat flux determines the stability of nucleate boiling. In a similar way the stability of film boiling can be discussed. Together these results explain in a qualitative way the familiar form of the boiling curve and the hysteresis of the transitions from nucleate to film boiling and back.

SAMENVATTING

Dit proefschrift beschrijft de resultaten van een onderzoek naar enkele interessante verschijnselen die optreden bij het koken van vloeistof in een vat. Ook bij ingewikkelder vormen van koken zijn deze verschijnselen van belang. De dampbellen worden gevormd in putjes in het verwarmingsoppervlak, zodat de groei plaatsvindt in de nabijheid van een vaste wand. Van de opeenvolgende fasen wordt die van snelle groei uitvoerig behandeld. Tijdens deze fase wordt de groeisnelheid bepaald door het warmtetransport naar de bel en neemt het belvolume met enkele orden van grootte toe. Een tweede onderwerp van studie vormt de overgang van kernkoken naar filmkoken bij hoge warmtestroomdichtheid. Hierbij wordt tussen de vloeistof en de wand een isolerende damp-laag gevormd.

Om deze verschijnselen te kunnen bestuderen hebben wij een doorzichtig verwarmingsoppervlak ontwikkeld. Op een plaat van geslepen glas of perspex werd als verwarmingselement een dunne elektrisch geleidende goudlaag opgedampt. De waarnemingen werden gedaan door een glazen prisma met behulp van een snelle filmcamera. Op deze wijze kon de aanwezigheid van dunne vloeistoflagen en droge plekken op het verwarmingsoppervlak worden aangetoond.

Het is bekend dat groeiende dampbellen bij lage druk de vorm van een halve bol hebben, waaronder op de vaste wand een dunne vloeistoflaag, de z.g. microlaag, aanwezig is. Verdamping van deze laag draagt bij tot het groeien van de bel. Bij het middelpunt van de bel is de laag geheel verdampt en vinden we een droge plek op de vaste wand. In onze experimenten waren deze verschijnselen direct waarneembaar. Uit proeven met de twee verschillende materialen voor het verwarmingsoppervlak kon een tweetal conclusies getrokken worden welke op het eerste gezicht met elkaar in tegenspraak waren. De groeisnelheid bleek nauwelijks van de thermische constanten van de wand af te hangen, maar de grootte van de droge plek nam sterk toe met de waarde van de contactcoëfficiënt van de vaste stof.

Op grond van een theoretische analyse toonden we aan dat deze vorm van groei beschreven wordt door een affiene oplossing. Zonder dat deze oplossing bepaald behoeft te worden, kan men op algemene gronden hieruit concluderen, dat de vorm van een bel niet verandert tijdens de groei en dat het kwadraat van de straal evenredig met de tijd toeneemt. De microlaag ontstaat doordat op de vaste wand onder de bel vloeistof uit de grenslaag achterblijft. Door te bewijzen dat deze grenslaag niet loslaat buiten de bel konden wij aantonen dat de vorming van zo'n microlaag mogelijk is. De nulde en eerste-orde termen voor de grenslaagdikte, die de dikte van de microlaag bepaalt, werden berekend.

Bij de beschrijving van de verdampende microlaag werd expliciet rekening gehouden met de warmteinhoud van de oververhitte vloeistof. De groeisnelheid en de straal van de droge plek werden numeriek berekend voor het geval waarin de contactcoëfficiënt van de vloeistof niet gelijk is aan die van de vaste stof. Een analytische oplossing kon worden verkregen voor het geval waarin de contactcoëfficiënten gelijk zijn.

Hoewel voor volledige verdamping van de microlaag een grote hoeveelheid warmte wordt geleverd door de vaste wand, blijkt uit de uitdrukking voor de groeisnelheid van de bel dat deze snelheid vrijwel geheel wordt bepaald door de initiële verdamping. Tijdens de initiële verdamping wordt nog uitsluitend warmte aan de vloeistof onttrokken. Dit verklaart waarom de belgroeisnelheid nauwelijks afhangt van de thermische constanten van de vaste wand, terwijl de straal van de droge plek wel sterk door deze constanten beïnvloed wordt. Hieruit blijkt tevens dat de analytische oplossing een bruikbare benadering verschaft voor het berekenen van de groeisnelheid, doch uiteraard niet voor de straal van de droge plek. De constante verhouding van de straal van de bel tot die van de droge plek, voorspeld op grond van het tijdens de groei niet veranderen van de belvorm, kon experimenteel worden aangetoond. De theoretische en experimentele waarden voor de groeisnelheid en de dikte van de microlaag stemden overeen.

Bij het naderen van de maximale warmtestroomdichtheid voor kernkoken kunnen vele plekken worden waargenomen waar het verwarmingsoppervlak gedurende korte tijd droog is. De meeste van deze droge plekken

verdwijnen weer, totdat plotseling een plek blijft groeien en de overgang naar filmkoken optreedt. Onze analyse van het thermisch onstabiele gedrag van zulke droge plekken is gebaseerd op een afwijkende interpretatie van het verband tussen warmteoverdracht en kookkromme. Wij vonden dat de eventuele voortgezette groei van de droge plekken afhangt van het al dan niet overschrijden van een kritische grootte. Het verband tussen deze kritische grootte en warmtestroomdichtheid bepaalt de stabiliteit van kernkoken. Een soortgelijke aanpak kan gebruikt worden voor de beschrijving van de stabiliteit van filmkoken. Tezamen verklaren deze resultaten op kwalitatieve wijze de bekende vorm van de kookkromme en het optreden van hysteresis bij de overgang van kernkoken naar filmkoken en omgekeerd.

LITERATURE

1. S.G. Bankoff, Chem. Engng. Progr. Symposium Series 29 (1959) 87.
2. P. Griffith, Symp. on boiling heat transfer in steam-generating units and heat exchangers, Manchester (1965). Nominated lecture.
3. S. Nukiyama, Journal Japan Soc. Mech. Engrs. 37 (1934) 367; English translation Int. J. Heat Mass Transfer 9 (1966) 1419.
4. C.J. Rallis and H.H. Jawurek, Int. J. Heat Mass Transfer 7 (1964) 1051.
5. Y.P. Chang, Trans. ASME 79 (1957) 1501.
6. L.J. Briggs, J. Appl. Phys. 19 (1948) 1062.
7. W.H. McAdams, "Heat Transmission", McGraw Hill, New York (1954) 370.
8. W.M. Rohsenow in "Developments in Heat Transfer", Ed. by W.M. Rohsenow, MIT Press Cambridge, Mass. (1964) 225.
9. N. Zuber, "Intern. Developments in Heat Transfer" (1961) 230. (Int. Heat Transfer Conference, Boulder, Colo.).
10. R. Siegel in "Advances in Heat Transfer", Volume 4, Ed. by J.P. Hartnett and Th. F. Irvine, Acad. Press New York (1967) 167.
11. W.J. Beek, Proc. Symp. on two-phase flow, Exeter (1965) F 401.
12. W.R. van Wijk, A.S. Vos and S.J.D. van Stralen, Chem. Engng. Sci. 5 (1956) 68.
13. S.J.D. van Stralen, Int. J. Heat Mass Transfer 9 (1966) 995.
14. L.E. Scriven, Chem. Engng. Sci. 10 (1959) 1.
15. J. Hovestreydt, Chem. Engng. Sci. 18 (1963) 631.
16. R.F. Gaertner, Trans. ASME Ser. C (1965) 17.
17. D.B. Kirby and J.W. Westwater, Chem. Engng. Progr. Symposium Series 57, (1965) 238.

18. R. Semeria and B. Martinet, Symp. on boiling heat transfer in steam generating units and heat exchangers, Manchester (1965) paper 3.
19. S.A. Kovalev, Int. J. Heat Mass Transfer 9 (1968) 1219.
20. H.K. Forster and N. Zuber, J. Appl. Phys. 25 (1954) 474.
21. M.S. Plesset and S.A. Zwick, J. Appl. Phys. 25 (1954) 493.
22. L.A. Waldman and G. Houghton, Chem. Engng. Sci. 20 (1965) 625.
23. G. Birkhoff, R.S. Margulies and W.A. Horning, Phys. Fluids 1 (1958) 201.
24. F.D. Moore and R.B. Mesler, A.I.Ch.E. Journal 7 (1961) 620.
25. S.J.D. van Stralen, Int. J. Heat Mass Transfer 9 (1966) 995.
26. Th.F. Rogers and R.B. Mesler, A.I.Ch.E. Journal 10 (1964) 656.
27. N.B. Hospeti and R.B. Mesler, A.I.Ch.E. Journal 11 (1965) 662.
28. C. Bonnet, E. Macke, R. Morin, Euratom Report EUR 1622 f (1964).
29. N. Madsen, Symp. on boiling heat transfer in steam-generating units and heat exchangers, Manchester (1965), paper 14.
30. R.R. Sharp, NASA TN D-1997 (1964).
31. R. Cole and H.L. Shulman, Int. J. Heat Mass Transfer 9 (1966) 1377.
32. V. Sernas and F.C. Hooper, Int. J. Heat Mass Transfer 12 (1969) 1627.
33. K.I. Torikai, Bull. JSME 10 (1967) 338.
34. K.I. Torikai and T. Yamazaki, Bull. JSME 10 (1967) 349.
35. M.G. Cooper and A.J.P. Lloyd, Int. J. Heat Mass Transfer 12 (1969) 895.
36. M.G. Cooper, Int. J. Heat Mass Transfer 12 (1969) 915.
37. Th.F. Mc Sweeney, Ph. D. thesis, Univ. of Michigan (1968).
38. R.R. Olander and R.G. Watts, Trans ASME, Ser. C, Jour. Heat Transfer 91 (1969) 178.

39. H.H. Jawurek, Int. J. Heat Mass Transfer 12 (1969) 843.
40. L.D. Landau and E.M. Lifshitz, "Fluid Mechanics", Pergamon Press, Oxford (1959) 51.
41. L.D. Landau and E.M. Lifshitz, "Fluid Mechanics", Pergamon Press, Oxford (1959) 81.
42. E.L. Knuth, Phys. Fluids 6 (1963) 321.
43. L.A. Skinner and S.G. Bankoff, Phys. Fluids 8 (1965) 1417.
44. K. Stephan, Brennstoff, Wärme, Kraft 17 (1965) 571.
45. S.J.D. van Stralen and W.M. Sluyter, Int. J. Heat Mass Transfer 12 (1969) 1353.

LIST OF SYMBOLS AND UNITS

a	heat diffusivity	$m^2 s^{-1}$
A } B }	auxiliary dimensionless functions	- -
c	specific heat	$J kg^{-1} K^{-1}$
C	dimensionless evaporation parameter	-
d	heating surface thickness	m
f	dimensionless modified stream function	-
g	acceleration of gravity	$m s^{-2}$
h	thickness of microlayer	m
h_0	original thickness of microlayer	m
h^*	displacement thickness of boundary layer	m
h_f	heat transfer coefficient for film boiling	$W m^{-2} K^{-1}$
h_n	heat transfer coefficient for nucleate boiling	$W m^{-2} K^{-1}$
H	ratio of heat diffusivities of solid and liquid	-
j	dimensionless stream function	-
J	dimensionless superheat	-
k	bubble growth constant	$m s^{-\frac{1}{2}}$
K	ratio of densities of liquid and vapour	-
L	latent heat of evaporation	$J kg^{-1}$
M	ratio of heat conductivities of solid and liquid	-
N	strength of heat source	W
p	pressure	$N m^{-2}$
$p(\infty)$	ambient pressure	$N m^{-2}$
P	Prandtl number of liquid	-
q	heat generation per unit surface area	$W m^{-2}$
Q	dimensionless pressure	-
r_b	bubble radius	m
r_c	nucleation radius	m

r_d	dry area radius	m
r_w	wire radius	m
R	Reynolds number	-
s_f	half length of dry area	m
s_n	half length of wetted area	m
S	surface area	m ²
t	time	s
T	temperature	K
T_0	saturation temperature at $p(\infty)$	K
T_1	initial temperature	K
T_c	maximum solid-liquid contact temperature	K
T_c^*	Leidenfrost temperature	K
v	velocity	m s ⁻¹
V	volume	m ³
w	dimensionless velocity	-
Z_b	dimensionless constant for microlayer thickness	-
α_b	dimensionless position of bubble surface	-
α_d	dimensionless dry area radius	-
β	} dimensionless thickness of microlayer	-
γ		-
θ	dimensionless temperature	-
λ	heat conductivity	Wm ⁻¹ K ⁻¹
μ	auxiliary parameter	m ⁻¹
ν	kinematic viscosity	m ² s ⁻¹
ρ	density	kgm ⁻³
ρ_v	saturated vapour density at temperature T_0	kgm ⁻³
ρ'_v	saturated vapour density at temperature T_1	kgm ⁻³
σ	surface tension	Nm ⁻¹
τ	dimensionless time	-
τ_d	dimensionless time for complete evaporation of microlayer	-
φ_b	stream function for boundary layer	m ³ s ⁻¹
Φ	local heat flux	Wm ⁻²
Φ_b	nucleate boiling peak heat flux	Wm ⁻²

ψ	angle between normal to bubble surface and radius vector	-
Ψ	vapour mass flux at bubble surface	$\text{kgm}^{-2}\text{s}^{-1}$
Ω	volumetric vapour flux at bubble surface	m s^{-1}
r	} spherical coordinates	m
θ		-
ϕ		-
α	dimensionless r-coordinate	-
\tilde{r}	} cylindrical coordinates	m
\tilde{z}		m
$\tilde{\phi}$		-
$\tilde{\alpha}$		dimensionless \tilde{r} -coordinate
$\tilde{\eta}$	} dimensionless \tilde{z} -coordinate	-
η		-
ξ		-

Indices

l	liquid
s	solid
v	vapour
f	film boiling
n	nucleate boiling

ACKNOWLEDGEMENTS

The research work described in this thesis was carried out at the Koninklijke/Shell Laboratorium Amsterdam (Shell Research N.V.). I express my gratitude to the management of the laboratory for their permission to use the results in this form and for the facilities offered for the preparation of my thesis. I believe that the inspiring discussions I had with many people, both in the laboratory and outside, have contributed greatly to my work. I am grateful to all those who actively supported me during its progress and to Dr. ir. H.L. Beckers in particular.

CURRICULUM VITAE

On completion of my HBS education in 1956 at 1^e Christelijk Lyceum in Haarlem I enrolled at Technische Hogeschool Delft as a physics student. In my fourth year I did research on a seismological model with Prof. O. Koefoed, in the last year on electron spin resonance with Prof. dr. B.S. Blaisse, to obtain my degree in October 1962.

My military service was done at "Verificatie van de Rijks Zee- en Luchtvaartinstrumenten", Wassenaar, from 1962 to 1964, where I held an advisory function for physical, especially optical, problems.

In 1964 I joined Koninklijke/Shell-Laboratorium Amsterdam. In the period from 1964 to 1967 the experiments described in this thesis were carried out there in the physics department which was headed by Dr. ir. H.L. Beckers. The theory of bubble growth developed in that period was cast in its present form during the first nine months of 1968, when I was a Visiting Fellow at University College in Cambridge, England. In Cambridge I worked on gas absorption with Prof. P.V. Danckwerts in the Department of Chemical Engineering.

H.J. van Ouwerkerk: "The role of the evaporating microlayer and dry surface areas in boiling"

ERRATA

page	line	present text	improved text
18	3 from bottom	$r_b \frac{dr_b^2}{dt^2}$	$r_b \frac{d^2 r_b}{dt^2}$
21	4 from top	Madsen ²⁷	Madsen ²⁹
21	5 from top	Van Stralen ²³	Van Stralen ²⁵
32	2 from top	(4.2.17)	(4.2.16)
34	12 from top	(4.2.27)	(4.2.17)
34	5 from bottom	(4.2.41)	(4.2.39)
39	3 from top	(4.2.41)	(4.2.42)
49	eq. (4.5.9)	-	+
52	6 from bottom	$-2a_{\ell} r_b \dots$	$-2\pi a_{\ell} r_b \dots$
89	1 from top	(6.2.31)	(6.2.32)
101	6 from top	<u>6</u> (1963) 321	<u>2</u> (1959) 84

STELLINGEN

1. In binaire mengsels is de groeisnelheid van een bel lager dan in een zuivere vloeistof. De reductie voor een bel groeiend aan een wand is bij goede benadering gelijk aan die voor een vrije bel.

L.E. Scriven,
Chem. Engng. Sci. 10 (1959) 1.

2. De door Cooper gevonden uitdrukkingen voor de groeisnelheid van een bel aan een vaste wand zijn niet juist.

M.G. Cooper,
Int. J. Heat Mass Transfer 12 (1969) 895.

3. De benadering die Olander en Watts gebruiken voor het berekenen van de grenslaagdikte van de stroming rondom een aan een wand groeiende bel geldt niet in de directe omgeving van deze bel.

R.R. Olander and R.G. Watts,
Trans. ASME, J. Heat Transfer 91 (1969) 178.

4. Concentratiegradiënten aan het oppervlak van de microlaag van een in een binair vloeistofmengsel groeiende bel, welke aanleiding kunnen geven tot oppervlaktespanningsgradiënten, treden alleen op nabij het middelpunt van de bel.

5. Tegen het hydrodynamische model dat gebruikt wordt om de overgang van kernkoken naar filmkoken te verklaren zijn verschillende bedenkingen aan te voeren.

N. Zuber,
Int. Dev. in Heat Transfer (1961) 230,
(Int. Heat Transfer Conference, Boulder, Colo.)

6. Veelal wordt stilzwijgend van de veronderstelling uitgegaan dat twee dampbellen op dezelfde wijze coalesceren als twee zeepbellen. Dit is niet juist.

G. Marucci,
Chem. Engng. Sci. 24 (1969) 975.

7. Voor een fysische slinger voorzien van een veer, die gebruikt kan worden voor het verkrijgen van een horizonindicatie aan boord van een rollend schip, kan een eenvoudig instelcriterium worden aangegeven.

8. De bevinding van Jenkins dat het turbulente Prandtl getal afneemt met toenemende waarde van het moleculaire Prandtl getal berust op een onjuiste interpretatie van resultaten uit de theorie der warmtegeleiding. Een juiste interpretatie van zijn model leidt tot het tegengestelde verloop.

R. Jenkins,
Proc. 1951 Heat Transfer and Fluid Mechanics Institute, Stanford, p. 147.

9. De door Schlichting beschreven methode voor het bepalen van het punt waar de grenslaag loslaat in een met de tijd veranderende stroming leidt tot een conceptuele moeilijkheid.

H. Schlichting,
"Grenzschicht-Theorie", Karlsruhe (1965), 391.

10. De bevinding dat de accumulatie van koolmonoxide in het bloed van verkeersagenten tijdens de dienst gering is wettigt niet de conclusie dat hoge concentraties van uitlaatgassen in de lucht ongevaarlijk zouden zijn.

A. de Bruin, A.R. Bult and A. van Haeringen,
T. Soc. Geneesk. 43 (1965) 775.

11. Indien een minimumsnelheid op autosnelwegen zou worden ingesteld dient overwogen te worden deze hoger te kiezen dan de snelheid waarbij de maximale capaciteit van de betrokken weg bereikt wordt.

12. De huidige praktijk waarbij de pensioenplichtige en de pensioengerechtigde leeftijd samenvallen moet als minder gewenst worden aangemerkt.

13. Alvorens wordt besloten voor de uitvoering van een civiel project een of meer fraaie bomen te rooien dient hun leeftijd te worden afgewogen tegen de geplande nuttige levensduur van het project.

14. Het is bekend dat de methode van Galerkin voor het benaderd oplossen van differentiaalvergelijkingen soms voordelen biedt ten opzichte van de methode van Ritz. In het geval van problemen waarbij de fysische constanten in de differentiaalvergelijking in aangrenzende gebieden verschillende waarden hebben, terwijl op de gemeenschappelijke rand aansluitingsvoorwaarden gelden, gaan deze voordelen verloren.